Journal of Applied and Computational Topology
https://doi.org/10.1007/s41468-023-00136-7

Sliding window persistence of quasiperiodic functions

Hitesh Gakhar[1] · **Jose A. Perea**[2]

Received: 10 November 2021 / Revised: 11 June 2023 / Accepted: 15 July 2023

Abstract
A function is called quasiperiodic if its fundamental frequencies are linearly independent over the rationals. With appropriate parameters, the sliding window point clouds of such functions can be shown to be dense in tori with dimension equal to the number of independent frequencies. In this paper, we develop theoretical and computational techniques to study the persistent homology of such sets. Specifically, we provide parameter optimization schemes for sliding windows of quasiperiodic functions, and present theoretical lower bounds on their Rips persistent homology. The latter leverages a recent persistent Künneth formula. The theory is illustrated via computational examples and an application to dissonance detection in music audio samples.

Keywords Topological data analysis · Persistent homology · Dynamical systems · Sliding window embeddings · Quasiperiodicity · Time series analysis

Mathematics Subject Classification Primary 55N31 · 37M10; Secondary 68W05

1 Introduction

Recurrent behavior—both in time and space—is ubiquitous in nature. *Periodicity* and *quasiperiodicity* are two prominent examples, characterized by a vector of underlying non-zero frequencies: If all pairwise ratios are rational, then the recurrence is periodic, while quasiperiodicity, on the other hand, occurs if there are at least two frequencies whose quotient is irrational. Quasiperiodic recurrence is at the heart of

✉ Hitesh Gakhar
hitesh.gakhar@gmail.com

Jose A. Perea
j.pereabenitez@northeastern.edu

[1] Department of Mathematics, University of Oklahoma, Norman, OK, USA

[2] Department of Mathematics and Khoury College of Computer Sciences, Northeastern University, Boston, MA, USA

Published online: 05 September 2023

KAM (Kolmogorov–Arnold–Moser) theory (Broer 2004), it appears as a signature of biphonation (i.e., the voicing of two simultaneous pitches) in mammalian vocalization (Wilden et al. 1998), in climate change patterns on Mars (Pollack and Toon 1982), in the oscillatory movement of the star TT Arietis (Hollander and Van Paradijs 1992), and in the brain functioning in mice as reported by fMRI scans (Belloy et al. 2017). The list goes on.

Quasiperiodicity in dynamical systems is typically studied with numerical methods including Birkhoff averages (Das et al. 2016), periodic approximations (Slater 1967; Sós 1958), estimation of Lyapunov exponents (Weixing et al. 1993), power spectra (Wojewoda et al. 1993), and recurrence quantification analysis (Webber and Zbilut 1994; Zbilut et al. 2002). New techniques from applied topology have emerged recently as complements to these traditional approaches in the task of recurrence detection—specifically for periodicity and quasiperiodicity quantification—in time series data (Perea and Harer 2015; Perea 2016; Tralie and Perea 2018). This novel framework combines two key ingredients: *sliding window embeddings* and *persistent homology*.

Sliding window (also known as time-delay) embeddings provide a framework to reconstruct the topology of state-space attractors in dynamical systems, given observed time series data. Indeed, given parameters $d \in \mathbb{N} = \{0, 1, \ldots\}$ (controlling the embedding dimension $d + 1$) and $\tau \in \{x \in \mathbb{R} \mid x > 0\}$ (the time delay) the sliding window embedding of $f : \mathbb{R} \longrightarrow \mathbb{C}$ at $t \in \mathbb{R}$ is the vector

$$SW_{d,\tau} f(t) := \begin{bmatrix} f(t) \\ f(t+\tau) \\ \vdots \\ f(t+d\tau) \end{bmatrix} \in \mathbb{C}^{d+1}. \tag{1}$$

The motivation behind this construction is Takens' embedding theorem (Takens 1981), which asserts that if f is the result of observing the evolution of a (potentially unknown) dynamical system, then the underlying topology of the sliding window point cloud $\mathbb{SW}_{d,\tau} f := SW_{d,\tau} f(\mathbb{R})$—generically in f and for appropriate parameters d, τ—recovers that of the traversed portion of the state space. In particular, this is how attractors can be reconstructed from observed time series data.

The topology of attractors constrains many properties of the underlying dynamical system (e.g., periodic orbits, chaos, etc) and detecting these features in practice is where persistent homology has come into play (Robins 1999). Persistent homology is a tool from Topological Data Analysis widely used to quantify multiscale homological features of shapes. Its typical input is a collection $\mathcal{K} = \{K_\epsilon\}_{\epsilon \geq 0}$ of spaces with $K_\epsilon \subset K_{\epsilon'}$ continuous for all $\epsilon \leq \epsilon'$. This is called a *filtration*. The output in each dimension $j \in \mathbb{N}$ is a multiset

$$\mathsf{dgm}_j(\mathcal{K}) \subset \{(x, y) \in [0, \infty] \times [0, \infty] \mid 0 \leq x < y\}$$

called the j-th *persistence diagram* of $\mathcal{K}$, where each pair $(a, b) \in \mathsf{dgm}_j(\mathcal{K})$ encodes a j-dimensional topological feature (like a connected component, a hole, or a void)

which appears at K_a and disappears entering K_b. The quantity $b-a$ is the *persistence* of the feature, and typically measures significance across the filtration.

In data analysis applications the input to persistent homology is often a metric space $(X, \mathbf{d}_X)$—e.g., a sliding window point cloud $\mathbb{SW}_{d,\tau} f$—from which the *Rips (simplicial) complex*

$$R_\epsilon(X, \mathbf{d}_X) := \left\{ \{x_0, \ldots, x_n\} \subset X \mid \max_{0 \le j,k \le n} \mathbf{d}_X(x_j, x_k) < \epsilon, \quad n \in \mathbb{N} \right\} \tag{2}$$

is computed at each scale $\epsilon \ge 0$, producing the *Rips filtration*

$$\mathcal{R}(X, \mathbf{d}_X) := \{R_\epsilon(X, \mathbf{d}_X)\}_{\epsilon \ge 0}. \tag{3}$$

Points in the Rips persistence diagrams $\mathsf{dgm}_j^{\mathcal{R}}(X) := \mathsf{dgm}_j\big(\mathcal{R}(X, \mathbf{d}_X)\big)$ quantify the underlying topology of X in that pairs (a, b) with large persistence $b-a$ represent likely topological features of a continuous space around which X accumulates.

The diagrams $\mathsf{dgm}_j^{\mathcal{R}}(\mathbb{SW}_{d,\tau} f)$ have shown to be rich signatures for recurrence detection in time series, with applications including: periodicity quantification in gene expression data (Perea et al. 2015), (quasi)periodicity detection in videos (Tralie and Perea 2018), synthesis of slow-motion videos from repetitive movements (Tralie and Berger 2018), wheezing detection (Emrani et al. 2014), and chatter prediction (Khasawneh et al. 2018). See Perea (2019) for a recent survey. One of the main challenges in these applications is the validation of empirical results, which stems, in part, from the current limited theoretical understanding of how $\mathsf{dgm}_j^{\mathcal{R}}(\mathbb{SW}_{d,\tau} f)$ depends on f, d, τ and T. That said, there are recent explicit conditions on f for $\mathbb{SW}_{d,\tau} f$ to provide appropriate reconstructions (Xu et al. 2019), as well as analyses of sliding window persistence for periodic functions (Perea and Harer 2015), and quasiperiodic functions of the form (Perea 2016)

$$f(t) = c_1 e^{it\omega_1} + \cdots + c_N e^{it\omega_N}. \tag{4}$$

In Eq. (4) the $\omega_n > 0$ are $\mathbb{Q}$-linearly independent (i.e., incommensurate), and the coefficients $c_n \in \mathbb{C}$ are nonzero. Our goal in this paper is to extend (Perea and Harer 2015) and (Perea 2016) to general quasiperiodic functions; i.e., those beyond Eq. (4).

1.1 Contributions

The first contribution of this paper is methodological: we develop techniques to study the persistent homology of sliding window point clouds from general quasiperiodic functions. Specifically, we show that if $f : \mathbb{R} \longrightarrow \mathbb{C}$ is quasiperiodic with incommensurate frequencies $\omega = (\omega_1, \ldots, \omega_N)$ (Definition 2.4), and if for $\mathbf{k} \in \mathbb{Z}^N$, $K \in \mathbb{N}$, we let

$$\widehat{F}(\mathbf{k}) = \lim_{\lambda \to \infty} \frac{1}{\lambda} \int_0^\lambda f(t) e^{-i\langle \mathbf{k}, t\omega \rangle} dt, \qquad S_K f(t) = \sum_{\|\mathbf{k}\|_\infty \le K} \widehat{F}(\mathbf{k}) e^{i\langle \mathbf{k}, t\omega \rangle}$$

then the Rips persistence diagrams $\mathsf{dgm}_j^{\mathcal{R}}(\mathbb{SW}_{d,\tau} f)$, $j \in \mathbb{N}$, can be approximated in bottleneck distance by $\mathsf{dgm}_j^{\mathcal{R}}(\mathbb{SW}_{d,\tau} S_K f)$ as $K \to \infty$. The diagrams of $\mathbb{SW}_{d,\tau} S_K f$ are then studied directly with methods extending those of Perea (2016), Perea and Harer (2015); the approximation to $\mathsf{dgm}_j^{\mathcal{R}}(\mathbb{SW}_{d,\tau} f)$ is of order $O\left(K^{\frac{N}{2}-r}\right)$ when $|\widehat{F}(\mathbf{k})| = O\left(\|\mathbf{k}\|_2^{-r}\right)$ and $r > N/2$ (Corollary 3.2).

This approximation strategy leads to our second contribution: computational schemes for optimizing the choice of parameters $d \in \mathbb{N}$ and $\tau > 0$, so that the geometry (and hence the Rips persistent homology) of the sliding window point cloud $\mathbb{SW}_{d,\tau} f = SW_{d,\tau} f(\mathbb{R})$ robustly reflects that of an N-torus. Explicitly:

1. Given f, estimate the coefficients $\widehat{F}(\mathbf{k})$ and their frequency locations $\langle \mathbf{k}, \omega \rangle$. This can be done numerically with methods leveraging the Discrete Fourier Transform (Gómez et al. 2010; Laskar 1993) or Wavelet analysis (Vela-Arevalo 2002).
2. Let $K \in \mathbb{N}$ be the smallest integer so that

$$\mathsf{supp}(\widehat{F}_K) := \left\{ \mathbf{k} \in \mathbb{Z}^N \mid \widehat{F}(\mathbf{k}) \neq 0 \text{ and } \|\mathbf{k}\|_\infty \leq K \right\}$$

   spans an N-dimensional $\mathbb{Q}$-vector space. This is possible provided f is smooth enough (Lemma 4.1).
3. Let d be the cardinality of $\mathsf{supp}(\widehat{F}_K)$, or alternatively, the number of prominent peaks in the spectrum of f. This choice is so that $\mathbb{SW}_{d,\tau} f$ has the right toroidal dimension (Theorem 4.2).
4. Let $\tau > 0$ be a minimizer over $[0, \tau_{\mathsf{max}}]$ of the scalar function

$$\Gamma(x) = \sum_{\mathbf{k} \neq \mathbf{k}'} \left| 1 + e^{ix\langle \mathbf{k}-\mathbf{k}', \omega \rangle} + \cdots + e^{ix\langle \mathbf{k}-\mathbf{k}', \omega \rangle d} \right|^2$$

   where the sum runs over $\mathbf{k}, \mathbf{k}' \in \mathsf{supp}(\widehat{F}_K)$. This choice is meant to amplify the toroidal features in $\mathsf{dgm}_j^{\mathcal{R}}(\mathbb{SW}_{d,\tau} f)$—see Figs. 4 and 5—and can be implemented via simple minimization algorithms.

Here, by toroidal features, we refer to the torus shaped attractors in the underlying dynamical system, which are captured by computing the persistent homology of the sliding window point cloud. By strong N-toroidal features, we mean that there are $\binom{N}{j}$ number of significant persistence points in $\mathsf{dgm}_j^{\mathcal{R}}$.

Our third contribution leverages the aforementioned approximation strategy, parameter choices, and a recent persistent Künneth formula (Gakhar and Perea 2019), to establish bounds for the cardinality and persistence of strong toroidal features in $\mathsf{dgm}_j^{\mathcal{R}}(\mathbb{SW}_{d,\tau} f)$, for $1 \leq j \leq N$. We prove the following (Sect. 6):

Theorem *With $K, d \in \mathbb{N}$ and $\tau > 0$ as before, let $\sigma_{\mathsf{min}} > 0$ be the smallest singular value of the $(d+1) \times d$ Vandermonde matrix $\left[e^{i\langle \mathbf{k}, \omega \rangle \tau j}\right]_{j=0,\ldots,d,\ \mathbf{k} \in \mathsf{supp}(\widehat{F}_K)}$. Moreover,*

let $\mathbf{k}_1, \ldots, \mathbf{k}_N \in \mathsf{supp}(\widehat{F}_K)$ *be* $\mathbb{Q}$*-linearly independent with*

$$|\widehat{F}(\mathbf{k}_1)| \geq |\widehat{F}(\mathbf{k}_2)| \geq \cdots \geq |\widehat{F}(\mathbf{k}_N)| > 0.$$

For $1 \leq n \leq N$*, let* $1 \leq n_1 < \cdots < n_\ell \leq N$ *be the longest sequence (i.e., largest* ℓ*) for which*

$$|\widehat{F}(\mathbf{k}_n)| = |\widehat{F}(\mathbf{k}_{n_1})| = \cdots = |\widehat{F}(\mathbf{k}_{n_\ell})|$$

and for $1 \leq j \leq N$*, let*

$$\mu_j(n) := \binom{n_1 - 1}{j - 1} + \cdots + \binom{n_\ell - 1}{j - 1}.$$

Then, there are at least $\mu_j(1) + \cdots + \mu_j(n)$ *toroidal features* $(a, b) \in \mathsf{dgm}_j^{\mathcal{R}}\left(\mathbb{SW}_{d,\tau} f\right)$*, counted with multiplicity, and with persistence*

$$b - a \;\geq\; \sqrt{3}|\widehat{F}(\mathbf{k}_n)|\sigma_{\mathsf{min}} \;-\; 4\sqrt{d+1}\|f - S_K f\|_\infty. \tag{5}$$

We envision for these kinds of theorems to be useful in separating noise from features in applications of quasiperiodicity detection/quantification with sliding windows and persistence. As an illustration, consider the quasiperiodic signal

$$f(t) = 2\sin(t) + 1.8\sin\left(\sqrt{3}t\right)$$

shown in Fig. 1 below (left), together with $\mathsf{dgm}_j^{\mathcal{R}}(\mathbb{SW}_{d,\tau} f)$ (right) in dimensions $j = 1$ (blue) and $j = 2$ (orange), computed with appropriate parameters d, τ. The corresponding theoretical lower bounds on persistence from Eq. (5) are depicted with dashed lines. We also use $f(t)$ to demonstrate the effect of random noise on sliding window persistence. See Sect. 7.1 for computational details.

Finally, as an application of the theory established in this paper, we illustrate how sliding windows and persistence can be used to identify the presence of dissonance in music audio recordings. Indeed, dissonant intervals in music (like *the tritone*) lead to quasiperiodic recurrence in the recorded audio waves, which we show can be effectively detected with the methods developed here. We also note that the preliminary versions of these results appeared in the first author's Ph.D. thesis (Gakhar 2020).

1.2 Organization

Section 2 presents the necessary mathematical background on the Fourier theory of quasiperiodic functions and persistent homology. Section 3 provides Fourier-type approximation theorems with explicit rates, at the level of sliding window point clouds and Rips persistent homology. Section 4 is devoted to studying the geometric structure of the sliding window point cloud $\mathbb{SW}_{d,\tau} S_K f$ as a function of the parameters involved.

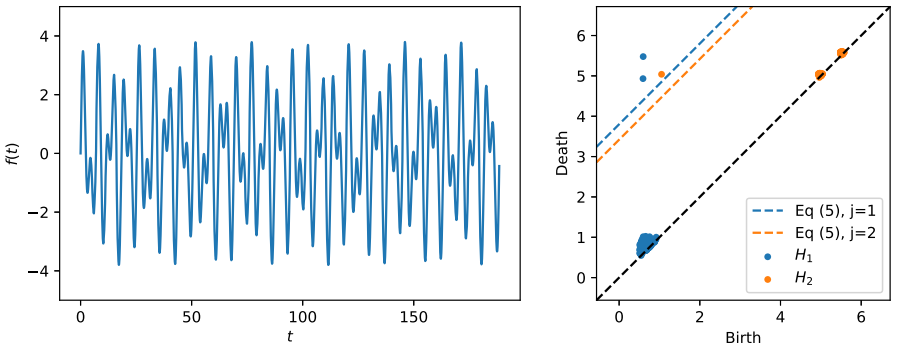

Fig. 1 Left: the function $f(t) = 2\sin(t) + 1.8\sin\left(\sqrt{3}t\right)$. Right: The persistence diagrams in dimensions $j = 1$ (blue) and $j = 2$ (orange) of the sliding window point cloud $\mathbb{SW}_{d,\tau} f$, together with the lower bounds on persistence (dashed lines) from Eq. (5) (color figure online)

In Sect. 5, we establish a computational framework for the optimization of d and τ. Section 6 establishes the advertised theoretical lower bounds on $\mathsf{dgm}_j^{\mathcal{R}}(\mathbb{SW}_{d,\tau} f)$, and we end in Sect. 7 with computational examples and applications.

1.3 Notation

Let $\mathbb{T} = \mathbb{R}/2\pi\mathbb{Z} \cong S^1$, that is, $[0, 2\pi]$ with the endpoints identified. Similarly for $N \in \mathbb{N}$, let $\mathbb{T}^N = (\mathbb{R}/2\pi\mathbb{Z})^N \cong S^1 \times \cdots \times S^1$. We will abuse notation and regard any $F : \mathbb{T}^N \longrightarrow \mathbb{C}$ as both a function of a variable $\mathbf{t} \in \mathbb{R}^N$ where each coordinate t_n is 2π-periodic, and also as a function on the quotient $\mathbb{T}^N$.

2 Preliminaries

In this section we establish the necessary background for later parts of the paper. In particular, we provide a short review of Kronecker's multidimensional approximation theorem in Sect. 2.1, as well as of quasiperiodic functions and their Fourier theory in Sect. 2.2. The theory of persistent homology is briefly discussed in Sect. 2.3.

2.1 Kronecker's theorem

If we regard $\mathbb{R}$ as a vector space over $\mathbb{Q}$, then a finite set $\{\beta_1, \ldots, \beta_N\} \subset \mathbb{R}$ is called *incommensurate* if $\beta_1, \ldots, \beta_N$ are linearly independent over $\mathbb{Q}$. That is, for $c_1, \ldots, c_N \in \mathbb{Q}$

$$c_1\beta_1 + \cdots + c_N\beta_N = 0 \quad \text{if and only if} \quad c_1 = \cdots = c_N = 0.$$

Kronecker's theorem is concerned with simultaneous diophantine approximations to real numbers, and incommensurability turns out to be the main condition. Later on we will use this theorem to see why sliding window point clouds from functions with

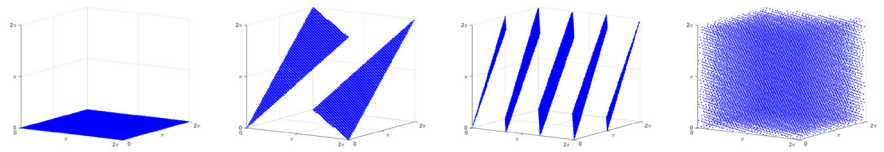

Fig. 2 The set $T\beta/2\pi\mathbb{Z}^3 \subset \mathbb{T}^3$ for $\beta = (\sqrt{2}, \sqrt{3}, 0)$ (left, a 2-torus), $\beta = (\sqrt{2}, \sqrt{3}, \sqrt{2}+\sqrt{3})$ (second, a 2-torus), $\beta = (\sqrt{2}, \sqrt{3}, 3\sqrt{2}+2\sqrt{3})$ (third, a 2-torus), $\beta = (\sqrt{2}, \sqrt{3}, \pi^2+1)$ (right, a 3-torus) and $T = \left[-10^4, 10^4\right] \cap \mathbb{Z}$

incommensurate frequencies (i.e., quasiperiodic) are dense in high-dimensional tori. For now, the theorem can be stated as follows (Apostol 2012, Chapter 7).

Theorem 2.1 (Kronecker) *$\{\beta_1, \ldots, \beta_N\} \subset \mathbb{R}$ is incommensurate if and only if for every $r_1, \ldots, r_N \in \mathbb{R}$ and every $\epsilon > 0$, there exist $t \in \mathbb{R}$ and $k_1, \ldots, k_N \in \mathbb{Z}$ so that*

$$|t\beta_n - r_n - 2\pi k_n| < \epsilon \qquad \text{for all} \qquad 1 \le n \le N. \tag{6}$$

As a consequence, the entries of $\beta = (\beta_1, \ldots, \beta_N) \in \mathbb{R}^N$ are incommensurate if and only if $\mathbb{R}\beta/2\pi\mathbb{Z}^N := \left\{t(\beta_1, \ldots, \beta_N) \mod 2\pi \mid t \in \mathbb{R}\right\}$ is dense in $\mathbb{T}^N$.

Remark 2.2 If one further assumes that $\{\pi, \beta_1, \ldots, \beta_N\}$ is incommensurate, then Eq. (6) holds with $t \in \mathbb{Z}$.

Here is a useful consequence of Kronecker's theorem:

Corollary 2.3 *Let $\beta = (\beta_1, \ldots, \beta_\alpha) \in \mathbb{R}^\alpha$, for $\alpha \in \mathbb{N}$. Then $\mathsf{span}_{\mathbb{Q}}\{\beta_1, \ldots, \beta_\alpha\}$ has dimension N over $\mathbb{Q}$, if and only if $\mathbb{R}\beta/2\pi\mathbb{Z}^\alpha \subset \mathbb{T}^\alpha$ is dense in an N-torus embedded in $\mathbb{T}^\alpha$.*

Before presenting the proof, and as an illustration of this Corollary, Fig. 2 shows what $T\beta/2\pi\mathbb{Z}^3$ looks like inside $\mathbb{T}^3$ for $T := \left[-10^4, 10^4\right] \cap \mathbb{Z}$ and β equals one of

$$\left(\sqrt{2}, \sqrt{3}, 0\right), \ \left(\sqrt{2}, \sqrt{3}, \sqrt{2}+\sqrt{3}\right), \ \left(\sqrt{2}, \sqrt{3}, 3\sqrt{2}+2\sqrt{3}\right), \ \left(\sqrt{2}, \sqrt{3}, \pi^2+1\right).$$

Notice that in each case, $T\beta/2\pi\mathbb{Z}^3$ traces a torus of the appropriate dimension, but embedded in ways governed by the linear relations between the entries of β.

Proof (of Corollary 2.3) Let $\{\beta_1, \ldots, \beta_\alpha\} \subset \mathbb{R}$ span an N-dimensional vector space over $\mathbb{Q}$, and without loss of generality, assume that $\beta_1, \ldots, \beta_N$ form a basis, $N < \alpha$. For $1 \le j \le \alpha - N$ let $k_j, k_{j,n} \in \mathbb{Z}$ be so that

$$k_j \beta_{N+j} = \sum_{n=1}^{N} k_{j,n} \beta_n \tag{7}$$

If $N = 1$ we further require that $\gcd(k_j, k_{j,1}) = 1$, and if $k = \mathrm{lcm}(k_1, \ldots, k_{\alpha-1})$, then it readily follows that

$$\begin{array}{ccc} \mathbb{T}^1 & \longrightarrow & \mathbb{T}^\alpha \\ t & \mapsto & \frac{kt}{\beta_1}\beta \end{array}$$

is an embedding of $\mathbb{T}^1$ into $\mathbb{T}^\alpha$ with the closure $\overline{\mathbb{R}\beta/2\pi\mathbb{Z}^\alpha} = \mathbb{R}\beta/2\pi\mathbb{Z}^\alpha$ as its image.

Now, for $N \geq 2$ define $\phi : \mathbb{R}^N \longrightarrow \mathbb{R}^\alpha$ and $\psi : \mathbb{R}^\alpha \longrightarrow \mathbb{R}^\alpha$ as

$$\phi(t_1, \ldots, t_N) = \left(t_1, \ldots, t_N, \sum_{n=1}^{N} k_{1,n} t_n, \ldots, \sum_{n=1}^{N} k_{\alpha-N,n} t_n \right) \tag{8}$$

$$\psi(t_1, \ldots, t_\alpha) = \left(t_1, \ldots, t_N, \, k_1 t_{N+1}, \ldots, \, k_{\alpha-N} t_\alpha \right) \tag{9}$$

Note that both ϕ and ψ preserve classes modulo 2π, and therefore descend to continuous maps $\phi : \mathbb{T}^N \longrightarrow \mathbb{T}^\alpha$, $\psi : \mathbb{T}^\alpha \longrightarrow \mathbb{T}^\alpha$. Moreover, since $\phi : \mathbb{T}^N \longrightarrow \mathbb{T}^\alpha$ is injective and tori are compact and Hausdorff, then ϕ is a homeomorphism onto its image. We claim that $\psi : \mathbb{T}^\alpha \longrightarrow \mathbb{T}^\alpha$ is injective when restricted to $\mathbb{R}\beta/2\pi\mathbb{Z}^\alpha$. Indeed, if $t \neq t' \in \mathbb{R}$ are so that $\psi(t\beta) = \psi(t'\beta)$ in $\mathbb{T}^\alpha$, then there exist $p, q \in \mathbb{Z}$ with

$$\begin{aligned} (t - t')\beta_1 &= 2\pi p \\ (t - t')\beta_2 &= 2\pi q \end{aligned}$$

which implies $q\beta_1 = p\beta_2$, contradicting the $\mathbb{Q}$-linear independence of $\beta_1, \ldots, \beta_N$. It follows that ψ is an injective continuous map on $\overline{\mathbb{R}\beta/2\pi\mathbb{Z}^\alpha}$, and thus induces a homeomorphism $\overline{\mathbb{R}\beta/2\pi\mathbb{Z}^\alpha} \cong \psi\left(\overline{\mathbb{R}\beta/2\pi\mathbb{Z}^\alpha}\right)$. Finally, since Eq. (7) implies that $\psi(t\beta) = \phi\big(t(\beta_1, \ldots, \beta_N)\big)$ for every $t \in \mathbb{R}$, and $\overline{(\beta_1, \ldots, \beta_N)/2\pi\mathbb{Z}^N} \cong \mathbb{T}^N$ by Kronecker's theorem, then

$$\overline{\mathbb{R}\beta/2\pi\mathbb{Z}^\alpha} \cong \psi\left(\overline{\mathbb{R}\beta/2\pi\mathbb{Z}^\alpha}\right) \cong \phi\left(\overline{(\beta_1, \ldots, \beta_N)/2\pi\mathbb{Z}^N}\right) = \phi\left(\mathbb{T}^N\right) \cong \mathbb{T}^N.$$

The only if direction follows from the fact that two tori of different dimensions cannot be homeomorphic. □

2.2 Quasiperiodic functions

As we alluded to in the introduction, quasiperiodic functions are superpositions of periodic oscillators with incommensurate frequencies. They arise in dynamical systems as observation functions on invariant toroidal submanifolds (Samoilenko 2012). More specifically,

Definition 2.4 Let $\omega_1, \ldots, \omega_N > 0$ be incommensurate. A function $f : \mathbb{R} \longrightarrow \mathbb{C}$ is said to be *quasiperiodic* with frequency vector $\omega = (\omega_1, \ldots, \omega_N)$ if

$$f(t) = F(\omega_1 t, \ldots, \omega_N t)$$

for all $t \in \mathbb{R}$ and a continuous function $F : \mathbb{T}^N \longrightarrow \mathbb{C}$. That is $F \in C(\mathbb{T}^N)$, which we will call a *parent function* for f.

Remark 2.5 The case $N = 1$ recovers the family of complex-valued periodic functions, and thus the results presented here generalize those of Perea and Harer (2015).

Remark 2.6 *(Important)* We will require throughout that the dimension N of the frequency vector $\omega \in \mathbb{R}^N$ for f quasiperiodic, be *minimal*. The reason being that if not, then a function like $f(t) = e^{i(1+\pi)t}$ can be regarded as being quasiperiodic with frequency vector $\omega = 1 + \pi$ and parent function $F(t) = e^{it}$, or as having $\omega = (1, \pi)$ for frequency vector and $F(t_1, t_2) = e^{i(t_1+t_2)}$ for parent function. Requiring that N be minimal, and showing that for a given ω the parent function is unique (we will do so in Theorem 2.7 below), eliminates this ambiguity.

It turns out that the traditional approximation theory via Fourier series on $L^2(\mathbb{T}^N)$ and $C(\mathbb{T}^N)$ can be leveraged to obtain similar insights for quasiperiodic functions. We describe how in what follows (Theorem 2.11), though the interested reader should also consult (Apostol 2012; Grafakos 2008; Samoilenko 2012). Indeed, let $\|(k_1, \ldots, k_N)\|_\infty = \max\limits_{1 \leq n \leq N} |k_n|$, and for $K \in \mathbb{N}$ let $I_K^N = \left\{\mathbf{k} \in \mathbb{Z}^N \mid \|\mathbf{k}\|_\infty \leq K\right\}$ be the integral square box of side $2K$. The K-truncated Fourier polynomial of $F \in L^2\left(\mathbb{T}^N\right)$ is the function

$$S_K F(\mathbf{t}) = \sum_{\mathbf{k} \in I_K^N} \widehat{F}(\mathbf{k}) e^{i\langle \mathbf{k}, \mathbf{t} \rangle} \tag{10}$$

where $\mathbf{t} = (t_1, \ldots, t_N) \in \mathbb{R}^N$, $\langle \cdot, \cdot \rangle$ is the standard inner product in $\mathbb{R}^N$, and

$$\widehat{F}(\mathbf{k}) = \frac{1}{(2\pi)^N} \int_0^{2\pi} \cdots \int_0^{2\pi} F(t_1, \ldots, t_N) e^{-i\langle \mathbf{k}, \mathbf{t} \rangle} dt_1 \cdots dt_N = \left\langle F, e^{i\langle \mathbf{k}, \cdot \rangle} \right\rangle_{L^2} \tag{11}$$

is the $\mathbf{k}$-Fourier coefficient of F, for $\mathbf{k} \in \mathbb{Z}^N$. As it is well-known (Grafakos 2008, Proposition 3.2.7), the sequence $\{S_K F\}_{K \in \mathbb{N}}$ converges to F in $L^2(\mathbb{T}^N)$ as $K \to \infty$. That is,

$$\lim_{K \to \infty} \|F - S_K F\|_{L^2} = 0.$$

It is not the case, however, that one has pointwise convergence $S_K F(\mathbf{t}) \to F(\mathbf{t})$, $\mathbf{t} \in \mathbb{T}^N$, even for $F \in C(\mathbb{T}^N)$ [see (Grafakos 2008, Proposition 3.4.6.) for negative results, and Theorem 2.9 below for appropriate conditions].

One can address these difficulties with *approximate identities*, and in particular using the *square Cesàro (or Fejér) mean*

$$C_K F(\mathbf{t}) = \sum_{\mathbf{k}\in I_K^N} \left(1 - \frac{|k_1|}{K+1}\right) \cdots \left(1 - \frac{|k_N|}{K+1}\right) \widehat{F}(\mathbf{k}) e^{i\langle \mathbf{k},\mathbf{t}\rangle} \tag{12}$$

which for $F \in C(\mathbb{T}^N)$ satisfies

$$\lim_{K\to\infty} \|F - C_K F\|_\infty = 0 \tag{13}$$

(this is Fejér's theorem) for $\|\cdot\|_\infty$ the sup-norm of uniform convergence in $C(\mathbb{T}^N)$. We now state the first main result on the Fourier theory of quasiperiodic functions.

Theorem 2.7 *If $f : \mathbb{R} \longrightarrow \mathbb{C}$ is quasiperiodic with frequency vector $\omega \in \mathbb{R}^N$, then f has a unique parent function $F \in C(\mathbb{T}^N)$ with Fourier coefficients*

$$\widehat{F}(\mathbf{k}) = \lim_{\lambda\to\infty} \frac{1}{\lambda} \int_0^\lambda f(t) e^{-i\langle \mathbf{k}, t\omega\rangle} dt. \tag{14}$$

Proof Write $f(t) = F(\omega t)$ for $F \in C(\mathbb{T}^N)$. Since $\lim_{K\to\infty} \|F - C_K F\|_\infty = 0$ (from Eq. (13)), then $C_K f(t) := C_K F(\omega t)$ converges to $f(t)$ uniformly in $t \in \mathbb{R}$. We claim that

$$\frac{1}{\lambda} \int_0^\lambda C_K f(t) e^{-i\langle \mathbf{k}, t\omega\rangle} dt \quad \to \quad \frac{1}{\lambda} \int_0^\lambda f(t) e^{-i\langle \mathbf{k}, t\omega\rangle} dt$$

uniformly in $\lambda > 0$ as $K \to \infty$. Indeed,

$$\left| \frac{1}{\lambda} \int_0^\lambda \big(C_K f(t) - f(t)\big) e^{-i\langle \mathbf{k}, t\omega\rangle} dt \right| \ \leq \ \|C_K f - f\|_\infty$$

where the right hand side goes to zero as $K \to \infty$ independent of λ. Therefore, by the Moore–Osgood theorem, we can exchange the order of limits as

$$\lim_{\lambda\to\infty} \frac{1}{\lambda} \int_0^\lambda f(t) e^{-i\langle \mathbf{k}, t\omega\rangle} dt = \lim_{K\to\infty} \lim_{\lambda\to\infty} \frac{1}{\lambda} \int_0^\lambda C_K f(t) e^{-i\langle \mathbf{k}, t\omega\rangle} dt \tag{15}$$

and if

$$\lambda_{\mathbf{k}} = \left(1 - \frac{|k_1|}{K+1}\right) \cdots \left(1 - \frac{|k_N|}{K+1}\right) \widehat{F}(\mathbf{k})$$

are the coefficients of $C_K F$ [defined in Eq. (12)], then evaluating the right hand side of Eq. (15) yields

$$\begin{aligned}\lim_{\lambda\to\infty}\frac{1}{\lambda}\int_0^\lambda f(t)e^{-i\langle\mathbf{k},t\omega\rangle}dt &= \lim_{K\to\infty}\lim_{\lambda\to\infty}\left(\lambda_{\mathbf{k}}+\sum_{\mathbf{k}'\in I_K^N\setminus\{\mathbf{k}\}}\lambda_{\mathbf{k}'}\frac{e^{i\langle\mathbf{k}'-\mathbf{k},\lambda\omega\rangle}-1}{i\langle\mathbf{k}'-\mathbf{k},\omega\rangle\lambda}\right)\\ &= \lim_{K\to\infty}\left(1-\frac{|k_1|}{K+1}\right)\cdots\left(1-\frac{|k_N|}{K+1}\right)\widehat{F}(\mathbf{k})\\ &= \widehat{F}(\mathbf{k}).\end{aligned}$$

If there were another parent function $G\in C(\mathbb{T}^N)$—i.e., with $f(t)=G(t\omega)$—then the above calculation shows that $\widehat{G}(\mathbf{k})=\widehat{F}(\mathbf{k})$ for every $\mathbf{k}\in\mathbb{Z}^N$. Since functions in $L^2(\mathbb{T}^N)$ with the same Fourier coefficients are equal almost everywhere (Grafakos 2008, Proposition 3.2.7), then continuity improves this to functional equality $G=F$. □

We now move onto providing conditions for the uniform convergence of

$$S_K f(t) := \sum_{\mathbf{k}\in I_K^N}\widehat{F}(\mathbf{k})e^{i\langle\mathbf{k},t\omega\rangle},\quad t\in\mathbb{R},\quad K\in\mathbb{N} \tag{16}$$

as $K\to\infty$. Here the $\widehat{F}(\mathbf{k})$ can be seen equivalently as the Fourier coefficients of the parent function F, or as the result of evaluating the right hand side of Eq. (14). The latter is what we expect to have access to in practice. We start with an upper bound on the size of the coefficients $\widehat{F}(\mathbf{k})$ (Grafakos 2008, Theorem 3.3.9).

Proposition 2.8 *Let $r\in\mathbb{N}$ and suppose that the partial derivatives $\partial^{\mathbf{l}}F$ exist and are continuous for all $\|\mathbf{l}\|_1=|l_1|+\cdots+|l_N|\le r$. That is, $F\in C^r(\mathbb{T}^N)$. Then*

$$\left|\widehat{F}(\mathbf{k})\right|\le\frac{\sqrt{N}^r}{\|\mathbf{k}\|_2^r}\left|\widehat{\partial_n^r F}(\mathbf{k})\right|$$

where $n=n(\mathbf{k})$ satisfies $|k_n|=\|\mathbf{k}\|_\infty$ and $\partial_n^r F$ is the r-th partial derivative of F with respect to t_n.

These types of inequalities can be used to estimate the degree r of regularity of the parent function F, by inspecting the rate of decay of the coefficients $\left|\widehat{F}(\mathbf{k})\right|$. Proposition 2.8 yields the following estimate for uniform approximation error.

Theorem 2.9 *If $F\in C^r(\mathbb{T}^N)$ for $\frac{N}{2}<r\in\mathbb{N}$, then*

$$\sum_{\mathbf{k}\notin I_K^N}\left|\widehat{F}(\mathbf{k})\right|\le\left(\frac{Area(\mathbb{S}^{N-1})N^r}{K^{2r-N}(2r-N)}\sum_{n=1}^N\left\|\partial_n^r F-S_K\partial_n^r F\right\|_{L^2}^2\right)^{1/2} \tag{17}$$

where $\partial_n^r F$ is the r-th partial derivative of F with respect to t_n. As a result, the sequence of Fourier coefficients $\widehat{F}(\mathbf{k})$ is absolutely summable, i.e.

$$\sum_{\mathbf{k}\in\mathbb{Z}^N} \left|\widehat{F}(\mathbf{k})\right| < \infty.$$

Proof From Proposition 2.8 we have that

$$\sum_{\mathbf{k}\notin I_K^N} \left|\widehat{F}(\mathbf{k})\right| \leq \sum_{\mathbf{k}\notin I_K^N} \frac{\sqrt{N}^r}{\|\mathbf{k}\|_2^r} \left|\widehat{\partial_n^r F}(\mathbf{k})\right| \tag{18}$$

for any fixed $K \in \mathbb{N}$. Note that $n = \underset{1\leq j\leq N}{\operatorname{argmax}} |k_j|$ depends on $\mathbf{k}$, so we will write it as $n(\mathbf{k})$, and the right hand side of Eq. (18) can be bounded using Cauchy-Schwarz as

$$\sum_{\mathbf{k}\notin I_K^N} \frac{\sqrt{N}^r}{\|\mathbf{k}\|_2^r} \left|\widehat{\partial_{n(\mathbf{k})}^r F}(\mathbf{k})\right| \leq \sqrt{N}^r \left(\sum_{\mathbf{k}\notin I_K^N} \frac{1}{\|\mathbf{k}\|_2^{2r}}\right)^{1/2} \left(\sum_{\mathbf{k}\notin I_K^N} \left|\widehat{\partial_{n(\mathbf{k})}^r F}(\mathbf{k})\right|^2\right)^{1/2}.$$

Moreover, since $\partial_n^r F$ is continuous and thus square integrable for each $n \in \mathbb{N}$, then its Fourier coefficients are square summable:

$$\sum_{\mathbf{k}\in\mathbb{Z}^N} \left|\widehat{\partial_n^r F}(\mathbf{k})\right|^2 = \left\|\partial_n^r F\right\|_{L^2}^2 < \infty \tag{19}$$

by Parseval's theorem. Hence, summing over n and rearranging terms we get

$$\sum_{\mathbf{k}\notin I_K^N} \left|\widehat{\partial_{n(\mathbf{k})}^r F}(\mathbf{k})\right|^2 \leq \sum_{n=1}^N \sum_{\mathbf{k}\notin I_K^N} \left|\widehat{\partial_n^r F}(\mathbf{k})\right|^2 = \sum_{n=1}^N \left\|\partial_n^r F - S_K \partial_n^r F\right\|_{L^2}^2$$

which goes to zero as $K \to \infty$. In order to bound the remaining sum of fractions, let $J_K^N = \left\{\mathbf{y} \in \mathbb{R}^N \;\middle|\; \|\mathbf{y}\|_\infty \leq K\right\}$ and let $B_K^N = \left\{\mathbf{y} \in \mathbb{R}^N \;\middle|\; \|\mathbf{y}\|_2 \leq K\right\}$. Observe that

$$\begin{aligned}\sum_{\mathbf{k}\notin I_K^N} \frac{1}{\|\mathbf{k}\|_2^{2r}} &\leq \int_{\mathbf{x}\notin J_K^N} \frac{1}{\left(y_1^2 + \cdots + y_N^2\right)^r} dy_1 \cdots dy_N \\ &\leq \int_{\mathbf{x}\notin B_K^N} \frac{1}{\left(y_1^2 + \cdots + y_N^2\right)^r} dy_1 \cdots dy_N\end{aligned}$$

which in higher dimensional spherical coordinates can be written as

$$\int_{\mathbb{S}^{N-1}} \int_{K}^{\infty} \frac{1}{\rho^{2r-N+1}} d\rho d\sigma$$

for $d\sigma$ the differential of surface area on the unit sphere $\mathbb{S}^{N-1}$ (the differential solid angle) and ρ the distance from a point in $\mathbb{R}^N$ to the origin. The integral satisfies

$$\begin{aligned}\int_{\mathbb{S}^{N-1}} \int_{K}^{\infty} \frac{1}{\rho^{2r-N+1}} d\rho d\sigma &= Area\left(\mathbb{S}^{N-1}\right) \frac{\rho^{N-2r}}{N-2r}\Big|_{K}^{\infty} \\ &= \frac{Area\left(\mathbb{S}^{N-1}\right)}{K^{2r-N}(2r-N)}\end{aligned}$$

and thus

$$\sum_{\mathbf{k}\notin I_K^N} \left|\widehat{F}(\mathbf{k})\right| \leq \left(\frac{Area(\mathbb{S}^{N-1})N^r}{K^{2r-N}(2r-N)} \sum_{n=1}^{N} \left\|\partial_n^r F - S_K \partial_n^r F\right\|_{L^2}^2\right)^{1/2}$$

where the right hand side goes to zero as $K \to \infty$. □

Remark 2.10 See Stein and Weiss (2016, Chapter VII, Corollary 1.9) for a result akin to Theorem 2.9. While both have similar hypotheses and deal with absolute Fourier convergence, Theorem 2.9 above gives explicit bounds for the size of the error term $\sum_{\mathbf{k}\notin I_Z^N} \left|\widehat{F}(\mathbf{k})\right|$. We will need such explicit estimates when discussing Fourier approximations to persistent homology of sliding window point clouds in Sect. 3.

Now, absolute summability of the Fourier coefficients $\widehat{F}(\mathbf{k})$ implies uniform convergence $S_K F \to F$, Stein and Weiss (2016, Chapter VII, Corollary 1.8), since

$$|F(\mathbf{t}) - S_K F(\mathbf{t})| \leq \sum_{\mathbf{k}\notin I_K^N} \left|\widehat{F}(\mathbf{k})\right|$$

for all $\mathbf{t} \in \mathbb{T}^N$. Combining this fact with Eq. (17), yields the following Fourier series approximation theorem for quasiperiodic functions:

Theorem 2.11 *Let f be quasiperiodic with parent function $F \in C^r(\mathbb{T}^N)$, $r > \frac{N}{2}$. If $S_K f$ is defined as in Eq. (16), then*

$$\|f - S_K f\|_\infty \leq \left(\frac{Area(\mathbb{S}^{N-1})N^r}{K^{2r-N}(2r-N)} \sum_{n=1}^{N} \left\|\partial_n^r F - S_K \partial_n^r F\right\|_{L^2}^2\right)^{1/2}$$

which goes to zero faster than $\frac{1}{K^{r-\frac{N}{2}}}$ as $K \to \infty$.

2.3 Persistent homology

As we mentioned in Sect. 1, persistent homology is a tool from Topological Data Analysis used to study the evolution of topological features in filtered spaces. Indeed, for any filtration $\mathcal{K} = \{K_\epsilon\}_{\epsilon \geq 0}$, taking homology in dimension $j \in \mathbb{N}$ and coefficients in a field $\mathbb{F}$ yields a family

$$H_j(\mathcal{K}; \mathbb{F}) = \left\{ T_{\epsilon,\epsilon'} : H_j(K_\epsilon; \mathbb{F}) \longrightarrow H_j(K_{\epsilon'}; \mathbb{F}), \quad \epsilon \leq \epsilon' \right\}$$

of $\mathbb{F}$-vector spaces and linear transformations $T_{\epsilon,\epsilon'}$ induced by the inclusion maps $K_\epsilon \hookrightarrow K_{\epsilon'}$, for $\epsilon \leq \epsilon'$. The j-th *persistent homology groups* are

$$H_j^{\epsilon,\epsilon'}(\mathcal{K}; \mathbb{F}) := \mathsf{Img}\left(T_{\epsilon,\epsilon'}\right) \tag{20}$$

and their dimension over $\mathbb{F}$ are the *persistent Betti numbers*

$$\beta_j^{\epsilon,\epsilon'}(\mathcal{K}) := \mathsf{rank}(T_{\epsilon,\epsilon'}) = \mathsf{dim}_{\mathbb{F}}\left(H_j^{\epsilon,\epsilon'}(\mathcal{K}; \mathbb{F})\right). \tag{21}$$

If $\beta_j^{\epsilon,\epsilon}(\mathcal{K}) < \infty$ for every ϵ—i.e., if $H_j(\mathcal{K}; \mathbb{F})$ is *pointwise-finite*—then a theorem of Crawley-Boevey (2015) contends that the isomorphism type of $H_j(\mathcal{K}; \mathbb{F})$ is uniquely determined by a multiset of intervals $I \subset [0, \infty]$, called the *barcode* of $H_j(\mathcal{K}; \mathbb{F})$, and denoted $\mathsf{bcd}_j(\mathcal{K})$. The (undecorated) *persistence diagram* $\mathsf{dgm}_j(\mathcal{K})$, on the other hand, is the multiset of pairs (a, b) resulting from taking the endpoints $a \leq b$ of the intervals in $\mathsf{bcd}_j(\mathcal{K})$. In terms of persistent Betti numbers, one can check that

$$\beta_j^{\epsilon,\epsilon'}(\mathcal{K}) = \#\left\{ I \in \mathsf{bcd}_j(\mathcal{K}) \;\mid\; [\epsilon, \epsilon'] \subset I \right\} \tag{22}$$

where cardinality (#) on the right hand side is that of multisets. If all intervals in $\mathsf{bcd}_j(\mathcal{K})$ are of the same type (i.e., all open, closed, right/left open), then

$$\beta_j^{\epsilon,\epsilon'}(\mathcal{K}) = \#\left\{ (a, b) \in \mathsf{dgm}_j(\mathcal{K}) \;\mid\; a \prec_\ell \epsilon \leq \epsilon' \prec_r b \right\} \tag{23}$$

where $\prec_\ell$ and $\prec_r$ are chosen to coincide with the interval type of $\mathsf{bcd}_j(\mathcal{K})$.

The pointwise-finite hypothesis on $H_j(\mathcal{K}; \mathbb{F})$ can be relaxed to $\beta_j^{\epsilon,\epsilon'}(\mathcal{K}) < \infty$ for all $\epsilon < \epsilon'$; this is called being q-*tame*, and is a condition satisfied by the persistent homology of the Rips filtration (defined in Eq. (3)) of any totally bounded metric space (Chazal et al. 2014, Proposition 5.1). It is known that barcodes and persistence diagrams can be defined in the q-tame case in such a way that Eq. (22) (and also Eq. (23) if all intervals are of the same type) is still valid (Chazal et al. 2016, Corollary 3.8, Theorem 3.9). As a result, and when $(X, \mathbf{d}_X)$ is totally bounded, we have well-defined Rips persistence diagrams

$$\mathsf{dgm}_j^{\mathcal{R}}(X, \mathbf{d}_X) := \mathsf{dgm}_j(\mathcal{R}(X, \mathbf{d}_X))$$

for every $j \in \mathbb{N}$.

A bit more is true: these diagrams are well-behaved in the sense that they are stable under Gromov–Hausdorff perturbations on $(X, \mathbf{d}_X)$. Here is what this means. The *Hausdorff* distance in a metric space $(\mathbb{M}, \mathbf{d})$ between two bounded and non-empty subsets $X, Y \subset \mathbb{M}$ is defined as

$$\mathbf{d}_H^{\mathbb{M}}(X, Y) := \inf \left\{ \delta > 0 \mid X \subset Y^{(\delta)} \text{ and } Y \subset X^{(\delta)} \right\}.$$

Here $X^{(\delta)}$ (resp. $Y^{(\delta)}$) is the union of open balls in $\mathbb{M}$ of radius $\delta > 0$ centered at points in X (resp. Y). Also, when the ambient metric space is clear, the notation $\mathbf{d}_H^{\mathbb{M}}(X, Y)$ is simplified to $\mathbf{d}_H(X, Y)$. The *Gromov–Hausdorff distance*, on the other hand, is defined for bounded metric spaces $(X, \mathbf{d}_X)$, $(Y, \mathbf{d}_Y)$ as

$$\mathbf{d}_{GH}\left((X, \mathbf{d}_X), (Y, \mathbf{d}_Y)\right) := \inf_{\mathbb{M}, \varphi, \psi} \mathbf{d}_H^{\mathbb{M}}\big(\varphi(X),\ \psi(Y)\big)$$

where the infimum runs over all metric spaces $(\mathbb{M}, \mathbf{d})$, and all isometric embeddings $\varphi : (X, \mathbf{d}_X) \hookrightarrow (\mathbb{M}, \mathbf{d})$, $\psi : (Y, \mathbf{d}_Y) \hookrightarrow (\mathbb{M}, \mathbf{d})$. In particular, if $X, Y \subset (\mathbb{M}, \mathbf{d})$, then

$$\mathbf{d}_{GH}((X, \mathbf{d}|_X), (Y, \mathbf{d}|_Y)) \leq \mathbf{d}_H^{\mathbb{M}}(X, Y). \tag{24}$$

The Gromov–Hausdorff distance is a measure of similarity between bounded metric spaces; in fact it is a pseudometric, which is zero if and only if the completions of the metric spaces involved are isometric. The stability of Rips persistence diagrams, on the other hand, is an inequality comparing the Gromov–Hausdorff distance between the input metric spaces, and a notion of distance between their persistence diagrams called the *bottleneck distance*. This distance is defined as follows: two persistence diagrams dgm and dgm' are said to be δ-matched, $\delta > 0$, if there is a bijection $\mu : A \longrightarrow A'$ of multisets $A \subset \mathsf{dgm}$ and $A' \subset \mathsf{dgm}'$ for which:

1. If $(x, y) \in A$ and $(x', y') = \mu(x, y)$, then $\max\left\{|x - x'|, |y - y'|\right\} < \delta$
2. If $(x, y) \in (\mathsf{dgm} \setminus A) \cup (\mathsf{dgm}' \setminus A')$ then $y - x < 2\delta$

The bottleneck distance between dgm and dgm' is

$$\mathbf{d}_B\big(\mathsf{dgm}, \mathsf{dgm}'\big) := \inf\left(\left\{\delta > 0 \mid \mathsf{dgm} \text{ and } \mathsf{dgm}' \text{ are } \delta - \text{matched } \right\} \cup \{\infty\}\right). \tag{25}$$

Finally, the stability of Rips persistent homology (Chazal et al. 2014, Theorem 5.2) contends that

$$\mathbf{d}_B\left(\mathsf{dgm}_j^{\mathcal{R}}(X, \mathbf{d}_X), \mathsf{dgm}_j^{\mathcal{R}}(Y, \mathbf{d}_Y)\right) \ \leq\ 2\mathbf{d}_{GH}\big((X, \mathbf{d}_X), (Y, \mathbf{d}_Y)\big) \tag{26}$$

for $(X, \mathbf{d}_X)$ and $(Y, \mathbf{d}_Y)$ totally bounded.

3 Fourier approximations of sliding window persistence

With the preliminaries out of the way, we now move onto studying the Rips persistent homology of sliding window point clouds from quasiperiodic functions. Thus far we have that if f is quasiperiodic and its parent function F has enough regularity, then f can be uniformly approximated by the truncated series $S_K f$. This is the content of Theorem 2.11, and in particular says that the higher the smoothness of F, then the faster the degree of approximation $S_K f \to f$. We will see next that these results can be readily bootstrapped to the level of sliding window point clouds, and hence to statements about Rips persistence diagrams.

Theorem 3.1 *Let f be quasiperiodic with parent function $F \in C^r(\mathbb{T}^N)$, $r > \frac{N}{2}$. If*

$$\mathbb{SW}_{d,\tau} f = SW_{d,\tau} f(T) \quad \text{and} \quad \mathbb{SW}_{d,\tau} S_K f = SW_{d,\tau} S_K f(T), \quad T \subset \mathbb{R}$$

are the sliding window point clouds of f and $S_K f$, respectively, then the Hausdorff distance between them satisfies

$$\begin{aligned} \mathbf{d}_H\left(\mathbb{SW}_{d,\tau} f\,,\, \mathbb{SW}_{d,\tau} S_K f\right) &\leq \sqrt{d+1}\|f - S_K\|_\infty \\ &\leq \left(\frac{Area(\mathbb{S}^{N-1})(d+1)N^r}{K^{2r-N}(2r-N)} \sum_{n=1}^{N} \left\| \partial_n^r F - S_K \partial_n^r F \right\|_{L^2}^2 \right)^{1/2} \end{aligned}$$

which goes to zero faster than $\frac{1}{K^{r-\frac{N}{2}}}$ as $K \to \infty$.

Proof Let $\epsilon > \sqrt{d+1}\|f - S_K f\|_\infty$, and let $t \in T$. Then

$$\|SW_{d,\tau} f(t) - SW_{d,\tau} S_K f(t)\|_2 \;\leq\; \sqrt{d+1}\|f - S_K f\|_\infty \;<\; \epsilon$$

which implies that ϵ satisfies both

$$\mathbb{SW}_{d,\tau} f \subset \left(\mathbb{SW}_{d,\tau} S_K f\right)^{(\epsilon)} \quad \text{and} \quad \mathbb{SW}_{d,\tau} S_K f \subset \left(\mathbb{SW}_{d,\tau} f\right)^{(\epsilon)}. \tag{27}$$

Since the Hausdorff distance in $\mathbb{C}^{d+1}$ between $\mathbb{SW}_{d,\tau} f$ and $\mathbb{SW}_{d,\tau} S_K f$ is the infimum over all $\delta > 0$ satisfying Eq. (27), then we have that

$$\mathbf{d}_H\left(\mathbb{SW}_{d,\tau} f\,,\, \mathbb{SW}_{d,\tau} S_K f\right) \;\leq\; \epsilon.$$

Because this is true for any $\epsilon > \sqrt{d+1}\|f - S_K f\|_\infty$, then

$$\mathbf{d}_H\left(\mathbb{SW}_{d,\tau} f\,,\, \mathbb{SW}_{d,\tau} S_K f\right) \leq \sqrt{d+1}\|f - S_K f\|_\infty$$

and the bound from Theorem 2.11 finishes the proof. □

Using the stability of Rips persistent homology (Eq. (26)), we can readily bound the bottleneck distance between the corresponding persistence diagrams:

Corollary 3.2 *With the same hypotheses of Theorem 3.1, and for all* $j \in \mathbb{N}$,

$$\begin{aligned}\mathbf{d}_B\left(\mathsf{dgm}_j^{\mathcal{R}}(\mathbb{SW}_{d,\tau} f), \mathsf{dgm}_j^{\mathcal{R}}(\mathbb{SW}_{d,\tau} S_K f)\right) &\leq 2\sqrt{d+1}\|f - S_K f\|_\infty \\ &\leq 2\left(\frac{Area(\mathbb{S}^{N-1})(d+1)N^r}{K^{2r-N}(2r-N)} \sum_{n=1}^{N} \left\|\partial_n^r F - S_K \partial_n^r F\right\|_{L^2}^2\right)^{1/2}\end{aligned}$$

and thus goes to zero faster than $\frac{1}{K^{r-\frac{N}{2}}}$ *as* $K \to \infty$.

The main point of these approximation results is that studying $\mathsf{dgm}_j^{\mathcal{R}}(\mathbb{SW}_{d,\tau} f)$ can be reduced to understanding $\mathsf{dgm}_j^{\mathcal{R}}(\mathbb{SW}_{d,\tau} S_K f)$ and its asymptotes as $K \to \infty$. This is a vastly more accessible simplification, as we will see shortly.

4 The geometric structure of $\mathbb{SW}_{d,\tau} S_K f$

Our next goal is to show that for suitable choices of $d, K \in \mathbb{N}$, $T \subset \mathbb{R}$, and $\tau > 0$, the closure of the sliding window point cloud $\mathbb{SW}_{d,\tau} S_K f = SW_{d,\tau} S_K f(T)$ in $\mathbb{C}^{d+1}$, is homeomorphic to an N-torus. Indeed, for $F \in C^r(\mathbb{T}^N)$ and $K \in \mathbb{N}$, let

$$\mathsf{supp}\left(\widehat{F}_K\right) = \left\{\mathbf{k} \in I_K^N \mid \widehat{F}(\mathbf{k}) \neq 0\right\}$$

denote the support of the Fourier transform $\widehat{F}$ restricted to the square box I_K^N.

Lemma 4.1 *Let* $f(t) = F(\omega t)$ *be quasiperiodic with frequency vector* $\omega \in \mathbb{R}^N$, *and parent function* $F \in C^r(\mathbb{T}^N)$, $r > \frac{N}{2}$. *Then, for all large enough* $K \in \mathbb{N}$, $\mathsf{supp}\left(\widehat{F}_K\right)$ *spans an* N*-dimensional* $\mathbb{Q}$*-vector space.*

Proof The first thing to note is that since

$$\mathsf{supp}\left(\widehat{F}\right) = \bigcup_{K \in \mathbb{N}} \mathsf{supp}\left(\widehat{F}_K\right) \subset \mathbb{Z}^N,$$

then $V = \mathsf{span}_{\mathbb{R}}\left(\mathsf{supp}\left(\widehat{F}\right)\right)$ is an $\mathbb{R}$-linear subspace of $\mathbb{R}^N$. It follows that

$$L = \mathsf{span}_{\mathbb{Z}}\left(\mathsf{supp}\left(\widehat{F}\right)\right)$$

is an additive discrete subgroup of V, and therefore a lattice (Stewart and Tall 2015, Theorem 6.1) of dimension $n \leq \mathsf{dim}_{\mathbb{R}}(V) \leq N$. It suffices to show that $n = N$.

Let $\mathbf{z}_1, \ldots, \mathbf{z}_n \in L$ be so that $L = \mathsf{span}_{\mathbb{Z}}\{\mathbf{z}_1, \ldots, \mathbf{z}_n\}$. Incommensurability of ω implies that $\tilde{\omega}_j = \langle \mathbf{z}_j, \omega \rangle$, $j = 1, \ldots, n$, are $\mathbb{Q}$-linearly independent, and we can assume without loss of generality that $\tilde{\omega}_j > 0$; otherwise replace $\mathbf{z}_j$ by $-\mathbf{z}_j$ as a

basis element for L. Hence, $\tilde{\omega} = (\tilde{\omega}_1, \ldots, \tilde{\omega}_n) \in \mathbb{R}^n$ is a vector of incommensurate frequencies.

For $\mathbf{t} \in \mathbb{T}^n$ let

$$G(\mathbf{t}) := \sum_{\mathbf{a} \in \mathbb{Z}^n} \widehat{F}(a_1\mathbf{z}_1 + \cdots + a_n\mathbf{z}_n) e^{i\langle \mathbf{a}, \mathbf{t} \rangle}$$

which converges uniformly in $\mathbf{t} \in \mathbb{T}^n$ since the Fourier coefficients $\widehat{F}(\mathbf{k})$ are absolutely summable (Theorem 2.9). Therefore $G \in C(\mathbb{T}^n)$, and thus

$$\begin{aligned} f(t) &= \sum_{\mathbf{k} \in \mathbb{Z}^N} \widehat{F}(\mathbf{k}) e^{i\langle \mathbf{k}, \omega \rangle t} \\ &= \sum_{\mathbf{a} \in \mathbb{Z}^n} \widehat{F}(a_1\mathbf{z}_1 + \cdots + a_n\mathbf{z}_n) e^{i\langle \mathbf{a}, \tilde{\omega} \rangle t} \\ &= G(\tilde{\omega} t) \end{aligned}$$

which shows that G is also a parent function for f, with $\tilde{\omega}$ as the corresponding frequency vector. Since the dimension N of the frequency vector for f is assumed to be minimal (Remark 2.6), then $n = N$, completing the proof. □

Now, if we write $\mathsf{supp}\left(\widehat{F}_K\right) = \{\mathbf{k}_1, \ldots, \mathbf{k}_\alpha\}$, for $1 \leq \alpha \leq (1 + 2K)^N$, then

$$SW_{d,\tau} S_K f(t) = \Omega_{K,f} \cdot x_{K,f}(t) \tag{28}$$

where

$$x_{K,f}(t) = \begin{bmatrix} \widehat{F}(\mathbf{k}_1) e^{i\langle \mathbf{k}_1, \omega \rangle t} \\ \vdots \\ \widehat{F}(\mathbf{k}_\alpha) e^{i\langle \mathbf{k}_\alpha, \omega \rangle t} \end{bmatrix} \in \mathbb{C}^\alpha \tag{29}$$

and $\Omega_{K,f}$ is the Vandermonde $(d+1) \times \alpha$ matrix

$$\Omega_{K,f} = \begin{bmatrix} 1 & \cdots & 1 \\ e^{i\langle \mathbf{k}_1, \omega \rangle \tau} & \cdots & e^{i\langle \mathbf{k}_\alpha, \omega \rangle \tau} \\ \vdots & & \vdots \\ e^{i\langle \mathbf{k}_1, \omega \rangle \tau d} & \cdots & e^{i\langle \mathbf{k}_\alpha, \omega \rangle \tau d} \end{bmatrix} \tag{30}$$

with nodes $e^{i\langle \mathbf{k}_1, \omega \rangle \tau}, \ldots, e^{i\langle \mathbf{k}_\alpha, \omega \rangle \tau} \in S^1 \subset \mathbb{C}$ (Aubel and Bölcskei 2019). We define $\mathbb{X}_{K,f}$ to be the collection of vectors $x_{K,f}(t)$ as above in Eq. (29):

$$\mathbb{X}_{K,f} = \left\{ x_{K,f}(t) \mid t \in \mathbb{R} \right\} \subset \mathbb{C}^\alpha. \tag{31}$$

The decomposition in Eq. (28) with Lemma 4.1 yields conditions on the parameters K, d, τ under which the sliding window point cloud $\mathbb{SW}_{d,\tau} S_K f$ is dense in a torus of the appropriate dimension. Indeed,

Theorem 4.2 *Let $f(t) = F(t\omega)$ be quasiperiodic with frequency vector $\omega \in \mathbb{R}^N$ and parent function $F \in C^r(\mathbb{T}^N)$, $r > \frac{N}{2}$. Let*

$$\mathsf{supp}(\widehat{F}_K) = \{\mathbf{k}_1, \ldots, \mathbf{k}_\alpha\}$$

and assume that $\tau > 0$ is not an integer multiple of $\frac{2\pi}{\langle \mathbf{k}_n - \mathbf{k}_m, \omega\rangle}$ for $1 \leq n < m \leq \alpha$. If $K \in \mathbb{N}$ is large enough so that $\mathsf{supp}(\widehat{F}_K)$ spans an N-dimensional $\mathbb{Q}$-vector space, and $d \geq \alpha - 1$, then the sliding window point cloud

$$\mathbb{SW}_{d,\tau} S_K f = SW_{d,\tau} S_K f(\mathbb{R})$$

is dense in an N-torus embedded in $\mathbb{C}^{d+1}$.

Proof The first thing to note is that since $\tau > 0$ is not an integer multiple of any $\frac{2\pi}{\langle \mathbf{k}_n - \mathbf{k}_m, \omega\rangle}$, $1 \leq n < m \leq \alpha$, then the points $e^{i\langle \mathbf{k}_1, \omega\rangle \tau}, \ldots, e^{i\langle \mathbf{k}_\alpha, \omega\rangle \tau} \in S^1$ are all distinct. Thus, the Vandermonde matrix $\Omega_{K,f}$ is full rank. This can be checked via induction on α, by showing that the determinant of an $\alpha \times \alpha$ Vandermonde matrix with nodes $\zeta_1, \ldots, \zeta_\alpha$ is $\prod_{1 \leq n < m \leq \alpha} (\zeta_m - \zeta_n)$. Combining this observation with $d + 1 \geq \alpha$, implies that $\Omega_{K,f} : \mathbb{C}^\alpha \longrightarrow \mathbb{C}^{d+1}$ is injective as a linear transformation.

Now, Corollary 2.3 with $\beta_1 = \langle \mathbf{k}_1, \omega\rangle, \ldots, \beta_\alpha = \langle \mathbf{k}_\alpha, \omega\rangle$, together with Lemma 4.1, imply that for all large enough $K \in \mathbb{N}$ the point cloud $\mathbb{X}_{K,f}$ (defined in Eq. (31)) is dense in an N-torus embedded in $\mathbb{C}^\alpha$. The result follows from $\Omega_{K,f}$ being a linear homeomorphism onto its image. □

Corollary 4.3 *With the same hypotheses of Theorem 4.2, and if $\{\pi, \omega_1, \ldots, \omega_N\}$ is incommensurate, then the sliding window point cloud*

$$\mathbb{SW}_{d,\tau} S_K f = SW_{d,\tau} S_K f(\mathbb{Z})$$

is dense in an N-torus embedded in $\mathbb{C}^{d+1}$.

Proof If $\mathbf{k}_1, \ldots, \mathbf{k}_N \in \mathbb{Z}^N$ are $\mathbb{Q}$-linearly independent, then incommensurability of $\{\pi, \omega_1, \ldots, \omega_N\}$ implies incommensurability of $\{\pi, \langle \mathbf{k}_1, \omega\rangle, \ldots, \langle \mathbf{k}_N, \omega\rangle\}$. The result follows in the same way as Theorem 4.2, but using the integer version of Kronecker's theorem as starting point (see Remark 2.2). □

We would like to emphasize that the condition on τ in Theorem 4.2 only guarantees the topology of an N-torus. Preserving the geometric structure as much as possible when going from $\mathbb{X}_{K,f}$ to $\mathbb{SW}_{d,\tau} S_K f$, and consequently amplifying the toroidal features in $\mathsf{dgm}_j^{\mathcal{R}}\left(\mathbb{SW}_{d,\tau} S_K f\right)$, requires specific optimizations on τ.

5 Parameter selection: how to optimize d and τ?

5.1 The embedding dimension

In practice, the diagrams

$$\mathsf{dgm}_j^{\mathcal{R}}\left(SW_{d,\tau}f(T)\right), \quad T \subset \mathbb{R} \text{ finite}$$

are computed as approximations to those of $SW_{d,\tau}f(\mathbb{R})$; the latter set is relatively compact, and hence the stability theorem (see Eq. (26)) implies that finite samples provide arbitrarily good approximations. The difficulty lies in that as $d \to \infty$, it becomes necessary for T to also grow in order to overcome the curse of (ambient space) dimensionality, and provide appropriate geometric recovery (Radovanovic et al. 2010). This is problematic since the Rips filtration grows exponentially in the number of points, and the matrix reduction algorithm for computing persistent homology is in the worst case cubic in the number of simplices (Morozov 2005). It is thus desirable for d to be as small as possible. With this and Theorem 4.2 in mind, we propose the following procedure for choosing d: Let K be the smallest integer so that $\mathsf{supp}(\widehat{F}_K)$ spans an N-dimensional vector space over $\mathbb{Q}$, and let d be the cardinality (α) of $\mathsf{supp}(\widehat{F}_K)$. When f is given numerically as a potentially noisy time series sampled at finitely many evenly spaced time points, then d can be estimated as the number of prominent peaks in the spectrum of f.

Remark 5.1 The structure theorems for both periodic functions (Perea and Harer 2015, Theorem 5.6) and quasiperiodic functions (Theorem 4.2) only require $d \geq \alpha - 1$. While the choice $d = \alpha - 1$ works for periodic signals in practice, we will demonstrate in Example 5.2 that $d = \alpha$ is preferable in the quasiperiodic case. This discrepancy arises in the computation of the time delay τ. Indeed, while for periodic functions there is a clear closed-form choice of τ, it turns out that this is typically not possible in the quasiperiodic case. We will investigate how in what follows.

5.2 The time delay

One way in which τ controls the shape of $\mathbb{SW}_{d,\tau}S_K f$ is via the condition number (i.e., the largest singular value divided by the smallest singular value) of the Vandermonde matrix $\Omega_{K,f}$ (defined in Eq. (30)). Indeed, when this number is much larger than 1 and the singular subspaces from the smallest singular values of $\Omega_{K,f}$ intersect $\overline{\mathbb{X}_{K,f}}$ transversally, then the persistence of the toroidal features of $\mathbb{SW}_{d,\tau}S_K f$ localized along these directions can be greatly diminished. One can avoid this problem by selecting a $\tau > 0$ promoting orthogonality between the columns $\mathbf{u}_1, \ldots, \mathbf{u}_\alpha$ of $\Omega_{K,f}$. Indeed, mutual orthogonality together with $\|\mathbf{u}_1\| = \cdots = \|\mathbf{u}_\alpha\| = \sqrt{d+1}$ would imply that $\Omega_{K,f}$ is $\sqrt{d+1}$ times a linear isometry. Such a transformation would have condition number equal to 1, and would preserve the persistent features of $\mathbb{X}_{K,f}$ (these are described in Theorem 6.6). That said, exact mutual orthogonally of the $\mathbf{u}_j$'s is not possible in general, for if $N \geq 3$, then $\langle \mathbf{u}_1, \mathbf{u}_2 \rangle = \langle \mathbf{u}_1, \mathbf{u}_3 \rangle = 0$ implies that there exist

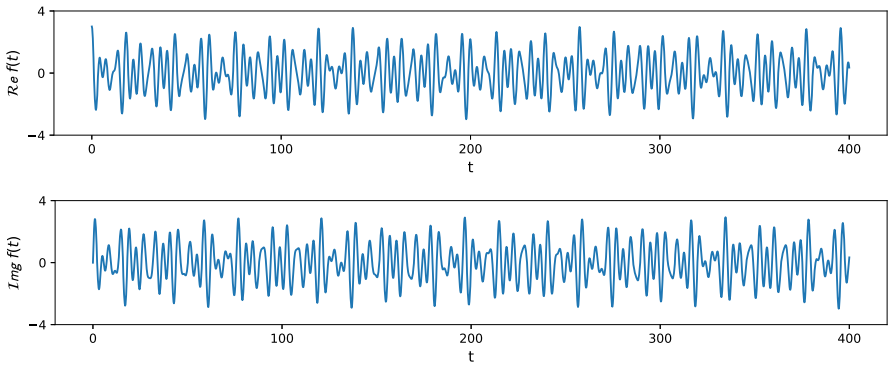

Fig. 3 Real (top) and imaginary (bottom) part of the function $f(t) = e^{it} + e^{i\sqrt{2}t} + e^{i\sqrt{3}t}$, $0 \le t \le 400$

$m, m' \in \mathbb{Z}$ satisfying

$$\langle \mathbf{k}_1 - \mathbf{k}_2, \omega \rangle \tau (d+1) = 2\pi m$$
$$\langle \mathbf{k}_1 - \mathbf{k}_3, \omega \rangle \tau (d+1) = 2\pi m'$$

which in turn would imply

$$m' \langle \mathbf{k}_1 - \mathbf{k}_2, \omega \rangle = m \langle \mathbf{k}_1 - \mathbf{k}_3, \omega \rangle$$

contradicting either the linear independence of $\mathbf{k}_1, \mathbf{k}_2, \mathbf{k}_3$, or the incommensurability of ω. We will settle for the next best option: to let τ be so that the $\mathbf{u}_j$'s are, in average, as orthogonal as possible. In other words, we will choose τ as a minimizer over $[0, \tau_{\mathsf{max}}]$ of the scalar function

$$\Gamma(x) := \sum_{1 \le j < \ell \le \alpha} \left| 1 + e^{i \langle \mathbf{k}_j - \mathbf{k}_\ell, \omega \rangle x} + \cdots + e^{i \langle \mathbf{k}_j - \mathbf{k}_\ell, \omega \rangle x d} \right|^2 \tag{32}$$

which is exactly the sum of squared magnitudes of the inner products $\langle \mathbf{u}_j, \mathbf{u}_\ell \rangle$ between the columns of the Vandermonde matrix $\Omega_{K,f}$. The thing to note is that when f is given as a noisy finite sample, then the inner products $\langle \mathbf{k}_j, \omega \rangle$ can be estimated as the frequency locations of the prominent peaks in the spectrum of f.

Example 5.2 As an illustration of our parameter selection procedure, let

$$f(t) = e^{it} + e^{i\sqrt{2}t} + e^{i\sqrt{3}t}, \quad 0 \le t \le 400.$$

The real and imaginary part of this function are shown in Fig. 3 below.
It can be readily checked that $\omega = \left(1, \sqrt{2}, \sqrt{3}\right)$ is the frequency vector for f, and

$$\mathsf{supp}(\widehat{F}_K) = \left\{(1,0,0), (0,1,0), (0,0,1)\right\}, \quad K \ge 1.$$

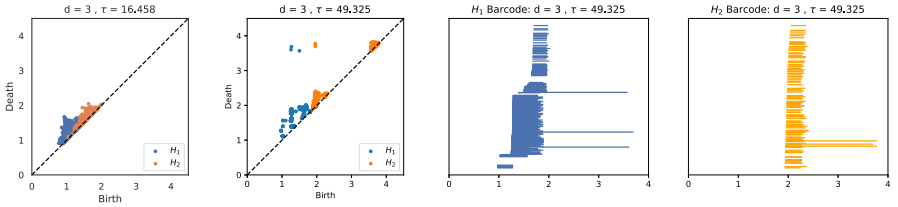

Fig. 4 Rips persistence diagrams of $SW_{d,\tau} f(T)$ in dimensions $j = 1$ (blue), $j = 2$ (orange), $\mathbb{F} = \mathbb{Z}_2$, $d = 3$, $\tau = 16.458$ (first) and $\tau = 49.325$ (second). Computations performed with `Ripser.py` (Tralie et al. 2018). We also provide the barcode representations in dim 1 (third) and dim 2 (fourth) to substantiate that there are indeed three strong classes in both dimensions (color figure online)

Following the discussion from Sect. 5.1 we let $d = 3$ (the cardinality of $\mathsf{supp}(\widehat{F}_K)$) and compute $\mathsf{dgm}_j^{\mathcal{R}}\left(SW_{d,\tau} f(T)\right)$ for $T \subset [0, 400]$ in dimensions $j = 1, 2$ as follows. We begin by evaluating $SW_{d,\tau} f(t)$ at 2,000 evenly spaced points in $[0, 400]$, and then further subsample this point cloud by selecting 800 points via `maxmin` sampling. That is, we pick $t_1 \in \widetilde{T} = \left\{\frac{n}{5} \mid n = 0, \ldots, 2000\right\}$ uniformly at random, and if $t_1, \ldots, t_\ell \in \widetilde{T}$ have been selected, then we let

$$t_{\ell+1} = \underset{t \in \widetilde{T}}{\text{argmax}} \ \min\left\{\|SW_{d,\tau} f(t) - SW_{d,\tau} f(t_1)\|, \ldots, \|SW_{d,\tau} f(t) - SW_{d,\tau} f(t_\ell)\|\right\}.$$

This inductive process continues until the sampling set $T = \{t_1, \ldots, t_{800}\} \subset \widetilde{T}$ is constructed, and then we compute the Rips persistence diagrams of $SW_{d,\tau} f(T)$ in dimensions $j = 1, 2$, coefficients in $\mathbb{Z}_2$, and two choices of time delay: $\tau = 16.458$ and $\tau = 49.325$. The resulting persistence diagrams are shown in Fig. 4 below.

We note that the `maxmin` sampling is used here because it selects subsample points in way that prevents clustering. This can be observed in the equation above: the time $t_{\ell+1}$ selected corresponds to the point $SW_{d,\tau} f(t_\ell)$ which is the farthest from the already chosen set $\{SW_{d,\tau} f(t_1), SW_{d,\tau} f(t_2), \ldots, SW_{d,\tau} f(t_\ell)\}$.

For this particular example we expect persistence diagrams consistent with a 3-torus—i.e., 3 strong classes in dimension 1, and 3 strong classes in dimension 2—since there are three linearly independent frequencies: 1, $\sqrt{2}$ and $\sqrt{3}$. That said, and as Fig. 4 shows, a poor choice of time delay (e.g., $\tau = 16.458$) can completely obscure these toroidal features with sampling artifacts (points near the diagonal). This stresses how important the need for delay optimization can be.

A broader picture of how the persistence of the top 3 features in each dimension varies with τ is shown in Fig. 5.

The value $\tau = 49.325$ is optimal in the sense that it jointly maximizes the persistence of the top 3 features in both dimensions. More importantly, it is also optimal in that it is a global minimizer over $[0, 100]$ for the function $\Gamma(x)$ (defined in Eq. (32)) as described in Sect. 5.2. We reiterate that the values $\langle \mathbf{k}, \omega \rangle$, $\mathbf{k} \in \mathsf{supp}(\widehat{F}_K)$, needed to compute τ as the minimizer of $\Gamma(x)$ can be estimated numerically as the frequency locations of the d most prominent peaks in the spectrum of f. Indeed, Fig. 6 shows the result of computing the Discrete Fourier Transform $\widehat{f}(\xi)$ of f sampled at $t \in \widetilde{T}$, as well as the locations of the most prominent peaks in amplitude.

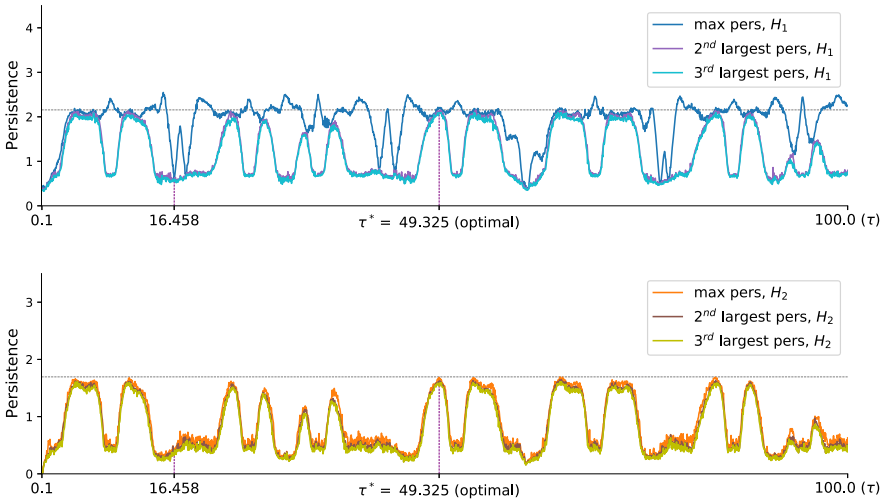

Fig. 5 Persistence of top 3 features in dimension 1 (top) and dimension 2 (bottom) as a function of τ, for $SW_{d,\tau} f(T)$ and $d = 3$

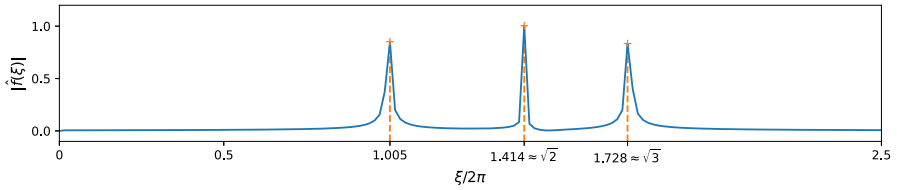

Fig. 6 Modulus of the discrete Fourier transform for f sampled at $t \in \widetilde{T}$. The locations of the most prominent peaks approximate the inner products $\langle \mathbf{k}, \omega \rangle$

An important thing to note is that the Discrete Fourier Transform (DFT) by itself is known to provide only very rough approximations to the frequency locations of quasiperiodic functions. This can have deleterious effects in the appropriate estimation of τ via minimization of $\Gamma(x)$. One solution is to use methods like (Gómez et al. 2010; Laskar 1993), which leverage the DFT to produce high-accuracy frequency estimates.

Finally, to illustrate the difference between the choices $d = \alpha$ and $d = \alpha - 1$ outlined in Remark 5.1, we repeat the same process above with $d = 2$. The persistence of the top 3 features in dimensions 1 and 2, as a function of τ, is shown in Fig. 7 below.

As Fig. 7 shows, the global minimizer $\tau = 65.731$ of $\Gamma(x)$, $0 \leq x \leq 100$, jointly maximizes the top 3 persistence values in both dimensions. In particular, the underlying 3-torus topology is clearly captured by this choice of time delay. One thing to note when comparing Fig. 5 ($d = \alpha = 3$) and Fig. 7 ($d = \alpha - 1 = 2$) is the number and nature of local maxima in persistence (specially in dimension 2) as a function of τ. Indeed, $d = 3$ yields a larger number of stable local maxima; by stable we mean that the values of persistence remain large in a neighborhood of a local maximizer. This suggests that while $d = 2$ still captures the right underlying topology, as Theorem 4.2 guarantees, the embedding in $\mathbb{C}^3$ of the sliding window point cloud is nonlinear

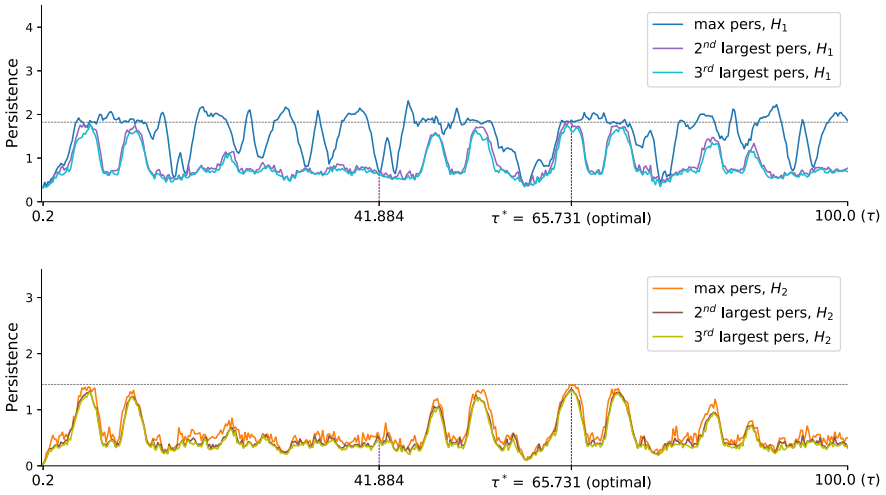

Fig. 7 Persistence of top 3 features in dimension 1 (top) and dimension 2 (bottom) as a function of τ, for $SW_{d,\tau} f(T)$ and $d = 2$

enough that strong features in persistence (with the ambient Euclidean distance) occur for only very specific time delays.

6 The rips persistent homology of $\mathbb{SW}_{d,\tau} S_K f$ and $\mathbb{SW}_{d,\tau} f$

We now turn our attention to the persistent homology of the sliding window point clouds $\mathbb{SW}_{d,\tau} S_K f$ and $\mathbb{SW}_{d,\tau} f$, as well as their dependence on both the Fourier coefficients $\widehat{F}(\mathbf{k})$, and the parameters K, d, τ. Our aim is to establish bounds on the cardinality and persistence of strong toroidal features in $\mathsf{dgm}_j^{\mathcal{R}}(\mathbb{SW}_{d,\tau} f)$. To that end, let $K \in \mathbb{N}$ be so that

$$\mathsf{supp}\left(\widehat{F}_K\right) = \{\mathbf{k}_1, \ldots, \mathbf{k}_\alpha\}, \qquad 1 \leq \alpha \leq (1+2K)^N$$

spans a $\mathbb{Q}$-vector space of dimension N (Lemma 4.1). We will further assume, after re-indexing if necessary, that $\mathbf{k}_1, \ldots, \mathbf{k}_N$ are $\mathbb{Q}$-linearly independent and that

$$|\widehat{F}(\mathbf{k}_1)| \geq |\widehat{F}(\mathbf{k}_2)| \geq \cdots \geq |\widehat{F}(\mathbf{k}_N)| > 0.$$

With this convention, let

$$\mathbb{T}^N_{\widehat{F}} := \left\{ \mathbf{z} \in \mathbb{C}^N \ : \ |z_1| = |\widehat{F}(\mathbf{k}_1)|, \ldots, |z_N| = |\widehat{F}(\mathbf{k}_N)| \right\} \tag{33}$$

regarded as a metric space with the $\|\cdot\|_\infty$ distance:

$$\|\mathbf{z} - \mathbf{z}'\|_\infty = \max\{|z_1 - z_1'|, \ldots, |z_N - z_N'|\}.$$

In order to understand the Rips persistent homology of $\mathbb{SW}_{d,\tau} f$, the first step is to clarify that of $\mathbb{T}^N_{\widehat{F}}$. This involves two theorems that we now describe. The first is a result by Adamaszek and Adams (2017, Theorem 7.4) computing the homotopy type of $R_\epsilon(S^1)$ at each scale $\epsilon > 0$.

Proposition 6.1 *(Adamaszek and Adams (2017)) The Rips complex $R_\epsilon(S^1_r)$ of a circle $S^1_r \subset \mathbb{C}$ of radius r (equipped with the Euclidean metric) is homotopy equivalent to $S^{2\ell+1}$ if and only if*

$$r_\ell = 2r \sin\left(\pi \frac{\ell}{2\ell+1}\right) \;<\; \epsilon \;\leq\; 2r \sin\left(\pi \frac{\ell+1}{2\ell+3}\right) = r_{\ell+1} \quad , \quad \ell \in \mathbb{N}.$$

Moreover, for all $\ell \in \mathbb{N}$ and $r_\ell < \epsilon \leq \epsilon' \leq r_{\ell+1}$, the inclusion $R_\epsilon(S^1_r) \hookrightarrow R_{\epsilon'}(S^1_r)$ is a homotopy equivalence.

As a consequence, the Rips persistent homology of $(S^1_r, |\cdot|)$ is pointwise-finite—hence q-tame—the resulting barcodes (and hence the persistence diagrams) are singleton multisets in odd dimensions, and empty in positive even dimensions:

$$\mathsf{bcd}_j^{\mathcal{R}}\left(S^1_r, |\cdot|\right) = \begin{cases} \left\{\left(2r \sin\left(\pi \frac{\ell}{2\ell+1}\right), 2r \sin\left(\pi \frac{\ell+1}{2\ell+3}\right)\right]\right\} & \text{if } j = 2\ell+1 \\ \{(0,\infty)\} & \text{if } j = 0 \\ \emptyset & \text{if } j = 2\ell+2 \end{cases} \tag{34}$$

The second result needed to describe $\mathsf{dgm}_j^{\mathcal{R}}(\mathbb{T}^N_{\widehat{F}}, \|\cdot\|_\infty)$ is a Künneth formula for Rips persistent homology and the maximum metric (Gakhar and Perea 2019, Corollary 4.6).

Proposition 6.2 *(Gakhar and Perea (2019)) Let $(X_1, \mathbf{d}_1), \ldots, (X_N, \mathbf{d}_N)$ be metric spaces with pointwise-finite Rips persistent homology. Then, for all $j \in \mathbb{N}$*

$$\mathsf{bcd}_j^{\mathcal{R}}(X_1 \times \cdots \times X_N, \mathbf{d}_{\mathsf{max}}) = \left\{ \bigcap_{n=1}^N I_{j_n} \;\middle|\; I_{j_n} \in \mathsf{bcd}_{j_n}^{\mathcal{R}}(X_n, \mathbf{d}_n),\ \sum_{n=1}^N j_n = j \right\}$$

and thus

$$\mathsf{dgm}_j^{\mathcal{R}}(X_1 \times \cdots \times X_N, \mathbf{d}_{\mathsf{max}}) = \left\{ \left(\max_n a_n, \min_n b_n\right) \;\middle|\; (a_n, b_n) \in \mathsf{dgm}_{j_n}^{\mathcal{R}}(X_n, \mathbf{d}_n),\ \sum_{n=1}^N j_n = j \right\}$$

where $\mathbf{d}_{\mathsf{max}}(\mathbf{x}, \mathbf{x}') := \max_{1 \leq n \leq N} \mathbf{d}_n(x_n, x'_n)$ is the maximum metric.

These results combined yield the following:

Lemma 6.3 *If* $a < \sqrt{3}|\widehat{F}(\mathbf{k}_N)|$, *then*

$$(a, b) \in \mathsf{dgm}_j^{\mathcal{R}}(\mathbb{T}^N_{\widehat{F}}, \|\cdot\|_\infty), \quad 1 \leq j \leq N$$

if and only if $a = 0$ *and* $b = \sqrt{3}|\widehat{F}(\mathbf{k}_n)|$ *for some* $1 \leq n \leq N$.

Moreover, if $1 \leq n \leq N$, *and* $1 \leq n_1 < \cdots < n_\ell \leq N$ *is the longest sequence (i.e., largest* ℓ*) for which*

$$|\widehat{F}(\mathbf{k}_n)| = |\widehat{F}(\mathbf{k}_{n_1})| = \cdots = |\widehat{F}(\mathbf{k}_{n_\ell})|$$

then $\left(0, \sqrt{3}|\widehat{F}(\mathbf{k}_n)|\right)$ *appears in* $\mathsf{dgm}_j^{\mathcal{R}}(\mathbb{T}^N_{\widehat{F}}, \|\cdot\|_\infty)$ *with multiplicity*

$$\mu_j(n) := \binom{n_1 - 1}{j - 1} + \cdots + \binom{n_\ell - 1}{j - 1}.$$

Proof By Proposition 6.2, we have that $(a, b) \in \mathsf{dgm}_j^{\mathcal{R}}(\mathbb{T}^N_{\widehat{F}}, \|\cdot\|_\infty)$, $1 \leq j \leq N$, if and only if there exist integers $0 \leq j_1, \ldots, j_N \leq j$ and

$$(a_n, b_n) \in \mathsf{dgm}_{j_n}^{\mathcal{R}}\left(S^1_{|\widehat{F}(\mathbf{k}_n)|}, |\cdot|\right), \quad 1 \leq n \leq N$$

so that $j_1 + \cdots + j_N = j$, $a = \max\{a_1, \ldots, a_N\}$ and $b = \min\{b_1, \ldots b_N\}$. Assume without loss of generality that $a = a_1$.

If

$$a_1 < \sqrt{3}|\widehat{F}(\mathbf{k}_N)| \leq \sqrt{3}|\widehat{F}(\mathbf{k}_1)|$$

then Eq. (34) implies that $a_1 = 0$ (hence $a_1 = \cdots = a_N = 0$) and therefore

$$b_n = \begin{cases} \infty & \text{if } j_n = 0 \\ \sqrt{3}|\widehat{F}(\mathbf{k}_n)| & \text{if } j_n = 1 \end{cases}, \quad \text{for all} \quad 1 \leq n \leq N.$$

The first part of the lemma readily follows from this and $j \geq 1$.

Let us now address the multiplicity computation. We will do so by counting the number of distinct copies of $\left(0, \sqrt{3}|\widehat{F}(\mathbf{k}_n)|\right)$ contributed to $\mathsf{dgm}_j^{\mathcal{R}}(\mathbb{T}^N_{\widehat{F}}, \|\cdot\|_\infty)$ by each index $1 \leq n_1 < \cdots < n_\ell \leq N$. Indeed, start with n_1 and assume $1 \leq j \leq n_1$. Then, each choice of $j - 1$ integers $1 \leq m_1 < \cdots < m_{j-1} < n_1$ yields a set of indices

$$\mathcal{M}(n_1) = \{m_1, \ldots, m_{j-1}, n_1\}$$

parametrizing a unique way of writing $\left(0, \sqrt{3}|\widehat{F}(\mathbf{k}_n)|\right)$ as $\left(\max_m a_m,\ \min_m b_m\right)$ for

$$(a_m, b_m) = \begin{cases} \left(0, \sqrt{3}|\widehat{F}(\mathbf{k}_m)|\right) & \text{if } m \in \mathcal{M}(n_1) \\ (0, \infty) & \text{if } m \in \{1, \ldots, N\} \setminus \mathcal{M}(n_1). \end{cases}$$

Since there are $\binom{n_1-1}{j-1}$ ways of choosing $\mathcal{M}(n_1)$, the sets $\mathcal{M}(n_1), \ldots, \mathcal{M}(n_\ell)$ are all distinct, and this computation accounts for all copies, then this completes the proof. □

Corollary 6.4 *If $0 < \delta \leq \epsilon < \sqrt{3}|\widehat{F}(\mathbf{k}_N)|$ and $1 \leq j \leq N$, then the homomorphism*

$$\iota_* : H_j\left(R_\delta(\mathbb{T}^N_{\widehat{F}}, \|\cdot\|_\infty); \mathbb{F}\right) \longrightarrow H_j\left(R_\epsilon(\mathbb{T}^N_{\widehat{F}}, \|\cdot\|_\infty); \mathbb{F}\right)$$

induced by the inclusion $\iota : R_\delta(\mathbb{T}^N_{\widehat{F}}, \|\cdot\|_\infty) \hookrightarrow R_\epsilon(\mathbb{T}^N_{\widehat{F}}, \|\cdot\|_\infty)$, is surjective.

Let

$$P : \mathbb{C}^\alpha \longrightarrow \mathbb{C}^N$$

be the projection onto the first N-coordinates. The first thing to note is that $P(\mathbb{X}_{K,f}) \subset \mathbb{T}^N_{\widehat{F}}$ (see Eq. (31)), and since

$$\|P(\mathbf{z}) - P(\mathbf{z}')\|_\infty \ \leq\ \|P(\mathbf{z}) - P(\mathbf{z}')\|_2 \ \leq\ \|\mathbf{z} - \mathbf{z}'\|_2$$

for every $\mathbf{z}, \mathbf{z}' \in \mathbb{C}^\alpha$, then P induces simplicial maps at the level of Rips complexes

$$\begin{array}{ccc} R_\epsilon(P) : R_\epsilon(\mathbb{X}_{K,f}, \|\cdot\|_2) & \longrightarrow & R_\epsilon(\mathbb{T}^N_{\widehat{F}}, \|\cdot\|_\infty) \\ \sigma & \mapsto & P(\sigma) \end{array}$$

for every $\epsilon > 0$. The idea now is to use $\mathcal{R}(P) = \{R_\epsilon(P) \mid \epsilon > 0\}$ in order to derive insights about the persistent homology of $\mathcal{R}(\mathbb{X}_{K,f}, \|\cdot\|_2)$ from that of $\mathcal{R}(\mathbb{T}^N_{\widehat{F}}, \|\cdot\|_\infty)$.

We have the following,

Lemma 6.5 *For all $0 < \epsilon < \sqrt{3}|\widehat{F}(\mathbf{k}_N)|$ and $1 \leq j \leq N$, the homomorphism*

$$R_\epsilon(P)_* : H_j(R_\epsilon(\mathbb{X}_{K,f}, \|\cdot\|_2); \mathbb{F}) \longrightarrow H_j(R_\epsilon(\mathbb{T}^N_{\widehat{F}}, \|\cdot\|_\infty); \mathbb{F})$$

is surjective.

Proof The case $N = 1$ is essentially Theorem 6.8 in Perea and Harer (2015), so assume $N \geq 2$.

Our first claim is that the projection $P : (\mathbb{C}^\alpha, \|\cdot\|_2) \longrightarrow (\mathbb{C}^N, \|\cdot\|_\infty)$ restricts to a homeomorphism

$$P : \overline{\mathbb{X}_{K,f}} \xrightarrow{\cong} \mathbb{T}^N_{\widehat{F}}$$

Indeed, surjectivity is the content of Kronecker's Theorem (2.1), so in order to check injectivity, assume that $\mathbf{x}, \mathbf{x}' \in \mathbb{X}_{K,f}$ have $P(\mathbf{x}) = P(\mathbf{x}')$, and write

$$\mathbf{x} = \begin{bmatrix} \widehat{F}(\mathbf{k}_1) e^{i\langle \mathbf{k}_1, \omega \rangle t} \\ \vdots \\ \widehat{F}(\mathbf{k}_\alpha) e^{i\langle \mathbf{k}_\alpha, \omega \rangle t} \end{bmatrix}, \quad \mathbf{x}' = \begin{bmatrix} \widehat{F}(\mathbf{k}_1) e^{i\langle \mathbf{k}_1, \omega \rangle t'} \\ \vdots \\ \widehat{F}(\mathbf{k}_\alpha) e^{i\langle \mathbf{k}_\alpha, \omega \rangle t'} \end{bmatrix}$$

for $t, t' \in \mathbb{R}$. Since $P(\mathbf{x}) = P(\mathbf{x}')$ and $\widehat{F}(\mathbf{k}_r) \neq 0$ for $r = 1, \ldots, \alpha$, then there exist $m_1, m_2 \in \mathbb{Z}$ for which

$$\begin{aligned} \langle \mathbf{k}_1, \omega \rangle (t - t') &= 2\pi m_1 \\ \langle \mathbf{k}_2, \omega \rangle (t - t') &= 2\pi m_2 \end{aligned}$$

If $t \neq t'$, then we would have that

$$\langle m_2 \mathbf{k}_1 - m_1 \mathbf{k}_2, \omega \rangle = 0$$

contradicting either the incommensurability of ω, or the $\mathbb{Q}$-linear independence of the vectors $\mathbf{k}_1, \mathbf{k}_2, \ldots, \mathbf{k}_N$. Thus $t = t'$, showing that P is injective on $\mathbb{X}_{K,f}$, and continuity plus Hausdorffness improves this to injectivity on $\overline{\mathbb{X}_{K,f}}$. Finally, since P provides a continuous bijection between $\overline{\mathbb{X}_{K,f}}$ and $\mathbb{T}^N_{\widehat{F}}$, and the former is compact (since it is closed and bounded), then P yields the desired homeomorphism.

Now, given $\epsilon > 0$, let $0 < \delta_\epsilon \leq \epsilon$ be so that

$$\| P(\mathbf{x}) - P(\mathbf{x}') \|_\infty < \delta_\epsilon \quad \text{always implies} \quad \| \mathbf{x} - \mathbf{x}' \|_2 < \epsilon \tag{35}$$

for $\mathbf{x}, \mathbf{x}' \in \mathbb{X}_{K,f}$. The existence of $\delta_\epsilon > 0$ follows from the uniform continuity of $P^{-1} : \mathbb{T}^N_{\widehat{F}} \longrightarrow \overline{\mathbb{X}_{K,f}}$, and replacing δ_ϵ with $\min\{\delta_\epsilon, \epsilon\}$ if necessary. Density of $\mathbb{X}_{K,f}$ in $\overline{\mathbb{X}_{K,f}}$ implies that for each $\mathbf{z} \in \mathbb{T}^N_{\widehat{F}}$ there is $\mathbf{x}_\mathbf{z} \in \mathbb{X}_{K,f}$ so that $\| P(\mathbf{x}_\mathbf{z}) - \mathbf{z} \|_\infty < \frac{\delta_\epsilon}{4}$. Fixing a choice of $\mathbf{x}_\mathbf{z}$ for each $\mathbf{z}$ defines a function

$$\begin{array}{rcl} \nu : \mathbb{T}^N_{\widehat{F}} & \longrightarrow & \mathbb{X}_{K,f} \\ \mathbf{z} & \mapsto & \mathbf{x}_\mathbf{z} \end{array}$$

satisfying

$$\| P \circ \nu(\mathbf{z}) - \mathbf{z} \|_\infty < \frac{\delta_\epsilon}{4}$$

for every $\mathbf{z} \in \mathbb{T}^N_{\widehat{F}}$. Therefore, if $\mathbf{z}, \mathbf{z}' \in \mathbb{T}^N_{\widehat{F}}$ are so that $\|\mathbf{z} - \mathbf{z}'\|_\infty < \frac{\delta_\epsilon}{2}$, then

$$\begin{aligned}\|P \circ \nu(\mathbf{z}) - P \circ \nu(\mathbf{z}')\|_\infty &\leq \|P \circ \nu(\mathbf{z}) - \mathbf{z}\|_\infty + \|\mathbf{z} - \mathbf{z}'\|_\infty + \|\mathbf{z}' - P \circ \nu(\mathbf{z}')\|_\infty \\ &< \frac{\delta_\epsilon}{4} + \frac{\delta_\epsilon}{2} + \frac{\delta_\epsilon}{4} \\ &= \delta_\epsilon\end{aligned}$$

which implies $\|\nu(\mathbf{z}) - \nu(\mathbf{z}')\|_2 < \epsilon$ (by Eq. (35)), and ν extends to a simplicial map

$$\begin{array}{rccc} R(\nu) : & R_{\frac{\delta_\epsilon}{2}}(\mathbb{T}^N_{\widehat{F}}, \|\cdot\|_\infty) & \longrightarrow & R_\epsilon(\mathbb{X}_{K,f}, \|\cdot\|_2) \\ & \sigma & \mapsto & \nu(\sigma) \end{array}$$

at the level of Rips complexes.

We claim that $R_\epsilon(P) \circ R(\nu)$ is contiguous to the inclusion

$$\iota : R_{\frac{\delta_\epsilon}{2}}(\mathbb{T}^N_{\widehat{F}}, \|\cdot\|_\infty) \hookrightarrow R_\epsilon(\mathbb{T}^N_{\widehat{F}}, \|\cdot\|_\infty)$$

Indeed, if $\mathbf{z}, \mathbf{z}' \in \mathbb{T}^N_{\widehat{F}}$ are so that $\|\mathbf{z} - \mathbf{z}'\|_\infty < \frac{\delta_\epsilon}{2}$, then

$$\begin{aligned}\|\mathbf{z}' - P \circ \nu(\mathbf{z})\|_\infty &\leq \|\mathbf{z}' - \mathbf{z}\|_\infty + \|P \circ \nu(\mathbf{z}) - \mathbf{z}\|_\infty \\ &< \frac{\delta_\epsilon}{2} + \frac{\delta_\epsilon}{4} \\ &< \delta_\epsilon \\ &\leq \epsilon\end{aligned}$$

showing that the set-theoretic union

$$\iota(\sigma) \ \cup \ \big(R_\epsilon(P) \circ R(\nu)\big)(\sigma)$$

is an element of $R_\epsilon(\mathbb{T}^N_{\widehat{F}}, \|\cdot\|_\infty)$ for every $\sigma \in R_{\frac{\delta_\epsilon}{2}}(\mathbb{T}^N_{\widehat{F}}, \|\cdot\|_\infty)$.

Contiguity at the level of simplicial maps implies that $\iota_* = R_\epsilon(P)_* \circ R(\nu)_*$ in homology, and since ι_* is surjective (Corollary 6.4), then it follows that $R_\epsilon(P)_*$ is also surjective. □

The next thing to note is that Lemma 6.3 together with Lemma 6.5 yields the following estimate for the number of toroidal persistent features in $\mathcal{R}(\mathbb{X}_{K,f}, \|\cdot\|_2)$:

Theorem 6.6 *Fix $1 \leq n \leq N$, and let $1 \leq n_1 < \cdots < n_\ell \leq N$ be the longest sequence for which*

$$|\widehat{F}(\mathbf{k}_n)| = |\widehat{F}(\mathbf{k}_{n_1})| = \cdots = |\widehat{F}(\mathbf{k}_{n_\ell})|.$$

Then, for each $1 \leq j \leq N$, *the multiset cardinality of*

$$\left\{(0,b) \in \mathsf{dgm}_j^{\mathcal{R}}\left(\mathbb{X}_{K,f}\right) \;\middle|\; b \geq \sqrt{3}|\widehat{F}(\mathbf{k}_n)|\right\}$$

is greater than or equal to $\mu_j(1) + \cdots + \mu_j(n)$, *for*

$$\mu_j(n) = \binom{n_1 - 1}{j-1} + \cdots + \binom{n_\ell - 1}{j-1}.$$

In order to make statements on $\mathsf{dgm}_j^{\mathcal{R}}(\mathbb{SW}_{d,\tau} S_K f)$, we will leverage the diagram

$$\left(\mathbb{SW}_{d,\tau} S_K f, \|\cdot\|_2\right) \underset{\Omega_{K,f}}{\overset{\Omega^+_{K,f}}{\rightleftarrows}} \left(\mathbb{X}_{K,f}, \|\cdot\|_2\right) \tag{36}$$

and the estimates in Rips persistence that it implies. Here $\Omega_{K,f}$ is the Vandermonde matrix defined in Eq. (30), and $\Omega^+_{K,f}$ is its Moore-Penrose pseudoinverse (see Ben-Israel and Greville (2003, III.3.4)).

Let $0 < \sigma_{\mathsf{min}} \leq \sigma_{\mathsf{max}}$ be the smallest and largest singular values of $\Omega_{K,f}$, respectively. Standard singular value decomposition arguments show that

$$\left\|\Omega_{K,f}\mathbf{u}\right\|_2 \leq \sigma_{\mathsf{max}}\|\mathbf{u}\|_2 \qquad \text{and} \qquad \left\|\Omega^+_{K,f}\mathbf{v}\right\|_2 \leq \frac{1}{\sigma_{\mathsf{min}}}\|\mathbf{v}\|_2$$

for every $\mathbf{u} \in \mathbb{C}^\alpha$ and $\mathbf{v} \in \mathbb{C}^{d+1}$, and thus we have induced simplicial maps

$$\begin{aligned}\Omega &: R_\epsilon(\mathbb{X}_{K,f}) \longrightarrow R_{\epsilon\sigma_{\mathsf{max}}}(\mathbb{SW}_{d,\tau} S_K f)\\ \Omega^+ &: R_{\delta\sigma_{\mathsf{min}}}(\mathbb{SW}_{d,\tau} S_K f) \longrightarrow R_\delta(\mathbb{X}_{K,f})\end{aligned}$$

at the level of Rips complexes. Let

$$\kappa(\Omega_{K,f}) = \frac{\sigma_{\mathsf{max}}}{\sigma_{\mathsf{min}}}$$

denote the condition number of $\Omega_{K,f}$. Then for every $\epsilon \leq \epsilon'$, the diagram

$$\begin{array}{ccccc} & & R_{\epsilon\sigma_{\mathsf{min}}}(\mathbb{SW}_{d,\tau} S_K f) & \hookrightarrow & R_{\epsilon'\sigma_{\mathsf{min}}}(\mathbb{SW}_{d,\tau} S_K f) \\ & \overset{\Omega}{\nearrow} & \downarrow{\scriptstyle \Omega^+} & & \downarrow{\scriptstyle \Omega^+} \\ R_{\epsilon/\kappa(\Omega_{K,f})}(\mathbb{X}_{K,f}) & \hookrightarrow & R_\epsilon(\mathbb{X}_{K,f}) & \hookrightarrow & R_{\epsilon'}(\mathbb{X}_{K,f}) \end{array} \tag{37}$$

commutes. The horizontal maps are inclusions, and commutativity follows from noting that $\Omega^+_{K,f}$ is a left inverse of $\Omega_{K,f}$. Indeed, the latter (tall skinny) matrix is full-rank with our choice of d and τ. Taking homology in dimension $j \in \mathbb{N}$ we get the induced homomorphisms

$$\begin{array}{ccc} & & H_j^{\epsilon\sigma_{\min},\,\epsilon'\sigma_{\min}}(\mathcal{R}(\mathbb{SW}_{d,\tau}S_K f);\mathbb{F}) \\ & & \downarrow \Omega^+_* \\ H_j^{\epsilon/\kappa(\Omega_{K,f}),\,\epsilon'}(\mathcal{R}(\mathbb{X}_{K,f});\mathbb{F}) & \hookrightarrow & H_j^{\epsilon,\,\epsilon'}(\mathcal{R}(\mathbb{X}_{K,f});\mathbb{F}) \end{array}$$

at the level of persistent homology groups (See Eq. (20)), where the horizontal map is an inclusion as linear spaces. Commutativity of the diagram in Eq. (37) implies that

$$H_j^{\epsilon/\kappa(\Omega_{K,f}),\,\epsilon'}(\mathcal{R}(\mathbb{X}_{K,f});\mathbb{F}) \subset \mathsf{Img}\left(\Omega^+_*\right)$$

which, after taking dimensions, yields the following inequality of persistent Betti numbers (see Eq. (21)):

$$\beta_j^{\epsilon\sigma_{\min},\,\epsilon'\sigma_{\min}}(\mathcal{R}(\mathbb{SW}_{d,\tau}S_K f)) \;\geq\; \mathsf{rank}\left(\Omega^+_*\right) \;\geq\; \beta_j^{\epsilon/\kappa(\Omega_{K,f}),\,\epsilon'}(\mathcal{R}(\mathbb{X}_{K,f}))$$

Letting $\epsilon \to 0$ and using Theorem 6.6, we get the following:

Theorem 6.7 *Let $f(t) = F(t\omega)$ be quasiperiodic with frequency vector $\omega \in \mathbb{R}^N$ and parent function $F \in C^r(\mathbb{T}^N)$, $r > \frac{N}{2}$. Fix parameters K, d, τ as before.*

Let $\sigma_{\min} > 0$ be the smallest singular value of the Vandermonde matrix $\Omega_{K,f}$ (see Eq. (30)), and for $1 \leq n \leq N$, let $1 \leq n_1 < \cdots < n_\ell \leq N$ be the longest sequence for which

$$|\widehat{F}(\mathbf{k}_n)| = |\widehat{F}(\mathbf{k}_{n_1})| = \cdots = |\widehat{F}(\mathbf{k}_{n_\ell})|.$$

Then, for each $1 \leq j \leq N$, the multiset cardinality of

$$\left\{(0,b) \in \mathsf{dgm}_j^{\mathcal{R}}\left(\mathbb{SW}_{d,\tau}S_K f\right) \;\middle|\; b \geq \sqrt{3}|\widehat{F}(\mathbf{k}_n)|\sigma_{\min}\right\}$$

is greater than or equal to $\mu_j(1) + \cdots + \mu_j(n)$ for

$$\mu_j(n) = \binom{n_1 - 1}{j-1} + \cdots + \binom{n_\ell - 1}{j-1}.$$

The Stability Theorem for Rips persistence (Eq. (26)), together with Theorem 6.7 and Corollary 3.2 yield the main result of this section.

Theorem 6.8 *With the same hypotheses of Theorem 6.7, and for $1 \leq j, n \leq N$, the multiset cardinality of*

$$\left\{(a,b) \in \mathsf{dgm}_j^{\mathcal{R}}\left(\mathbb{SW}_{d,\tau}f\right) \;\middle|\; b - a \;\geq\; \sqrt{3}|\widehat{F}(\mathbf{k}_n)|\sigma_{\min} - 4\sqrt{d+1}\|f - S_K f\|_\infty\right\}$$

is greater than or equal to $\mu_j(1) + \cdots + \mu_j(n)$.

The extremal singular values of Vandermonde matrices with nodes in the unit circle haven been extensively studied in the harmonic analysis and computational mathematics literature (Aubel and Bölcskei 2019; Moitra 2015; Ferreira 1999). In particular, the lower bound on $\sigma_{\min}$ from Aubel and Bölcskei (2019, Eq. (55)) implies the following.

Corollary 6.9 *With the same hypotheses of Theorem 6.7, and if*

$$d > \frac{1}{\delta_\omega} - \frac{3}{2}, \qquad \delta_\omega := \min_{1 \le \ell < m \le \alpha} \frac{1}{\pi} \arcsin\left(\frac{\left| e^{i\langle \mathbf{k}_\ell, \omega \rangle \tau} - e^{i\langle \mathbf{k}_m, \omega \rangle \tau} \right|}{2} \right)$$

then, for each $1 \le j, n \le N$, *the multiset cardinality of*

$$\left\{ (a,b) \in \mathsf{dgm}_j^{\mathcal{R}}\left(\mathbb{SW}_{d,\tau} f\right) \left| b - a \ge \sqrt{3} |\widehat{F}(\mathbf{k}_n)| \sqrt{d + \frac{3}{2} - \frac{1}{\delta_\omega}} - 4\sqrt{d+1} \| f - S_K f \|_\infty \right. \right\}$$

is always greater than or equal to $\mu_j(1) + \cdots + \mu_j(n)$.

This brings us to the end of the theoretical quasiperiodicity analysis in this paper. In the next section, we focus on examples and applications.

7 Experiments and applications

This section has two goals: first, to illustrate the pipeline developed in this paper for the analysis of quasiperiodic time series data. Indeed, we will utilize a synthetic example to review the optimization of d and τ, evaluate our theoretical lower bounds on persistence, and study the effects of noise on sliding window persistence. The second goal is to provide an example of how quasiperiodicity can arise in naturally-occurring time series data. Specifically, we will study a sound recording of *dissonance*, and illustrate how quasiperiodicity emerges through the lens of sliding windows and persistence.

7.1 Computational pipeline and valuation of theoretical lower bounds

Let

$$f(t) = 2\sin(t) + 1.8\sin\left(\sqrt{3}t\right) \quad \text{for} \quad 0 \le t \le 60\pi$$

with graph shown in Fig. 8 below.

We sample f at 10,000 evenly spaced points; that is, at each

$$t \in T = \left\{ \frac{3n\pi}{500} \mid n = 0, \ldots, 9,999 \right\}$$

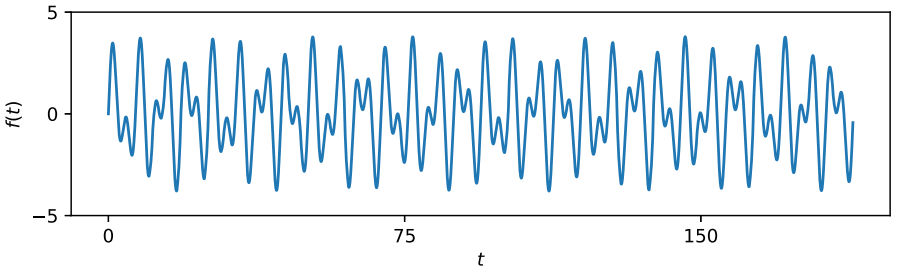

Fig. 8 $f(t) = 2\sin(t) + 1.8\sin\left(\sqrt{3}t\right)$ for $0 \le t \le 60\pi$

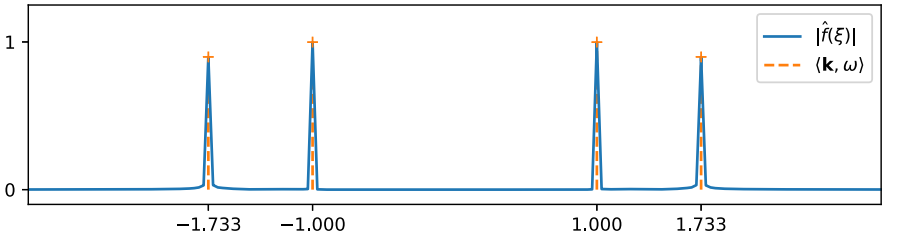

Fig. 9 Modulus of the DFT for $f(T)$

producing a discrete time series for which the Discrete Fourier Transform is computed (see Fig. 9 below). We note that since f is real-valued, then $|\widehat{f}(\xi)|$ is symmetric with respect to the origin, $\omega = \left(1, \sqrt{3}\right)$, $\mathbf{k}_1 = (1,0)$, $\mathbf{k}_2 = (0,1)$, $\mathbf{k}_3 = (-1,0)$, $\mathbf{k}_4 = (0,-1)$, and that $|\widehat{F}(\mathbf{k}_1)| = |\widehat{F}(\mathbf{k}_3)| \approx 1$, $|\widehat{F}(\mathbf{k}_2)| = |\widehat{F}(\mathbf{k}_4)| \approx 0.9$.

The number of prominent peaks in $|\widehat{f}(\xi)|$ is used—as described in Sect. 5.1—to select $d = 4$, while the peak locations $\langle \mathbf{k}, \omega \rangle$ define the function $\Gamma(x)$ (see Eq. (32)) whose minimizer over $[0, \tau_{\max}]$, for $\tau_{\max} = \frac{3}{4}\frac{60\pi}{d}$, yields the choice $\tau \approx 11.9577$ as described in Sect. 5.2. The value of $\tau_{\max}$ is selected to guarantee that the window size $d\tau$ is less than that of the domain T over which f is evaluated.

The number of points in T is already large enough that computing the Rips persistent homology of $SW_{d,\tau} f(T)$, using standard software (Bauer 2016), is algorithmically intensive. Thus, we take a `maxmin` subsample $SW_{d,\tau} f(\widetilde{T})$ (see Example 5.2) by selecting $\widetilde{T} \subset T$ with 1,000 points, and compute $\mathsf{dgm}_j^{\mathcal{R}}\left(SW_{d,\tau} f(\widetilde{T})\right)$ in dimensions $j = 1, 2$ and coefficients in $\mathbb{F} = \mathbb{Z}_2$.

Since $\widetilde{T} \neq \mathbb{R}$, then the lower bounds on persistence from Theorem 6.7 do not readily apply to the diagrams $\mathsf{dgm}_j^{\mathcal{R}}(SW_{d,\tau} f(\widetilde{T}))$. That said, the stability theorem implies that the inequality can be corrected to

$$b - a \;\ge\; \sqrt{3}|\widehat{F}(\mathbf{k}_n)|\sigma_{\min} - 4\sqrt{d+1}\|f - S_K f\|_\infty - 4d_H\left(SW_{d,\tau} f(\widetilde{T}), \mathbb{SW}_{d,\tau} f\right) \tag{38}$$

where, for this example, the Hausdorff distance term was estimated as

$$d_H\left(SW_{d,\tau} f(\widetilde{T}), \mathbb{SW}_{d,\tau} f\right) \approx 0.54292.$$

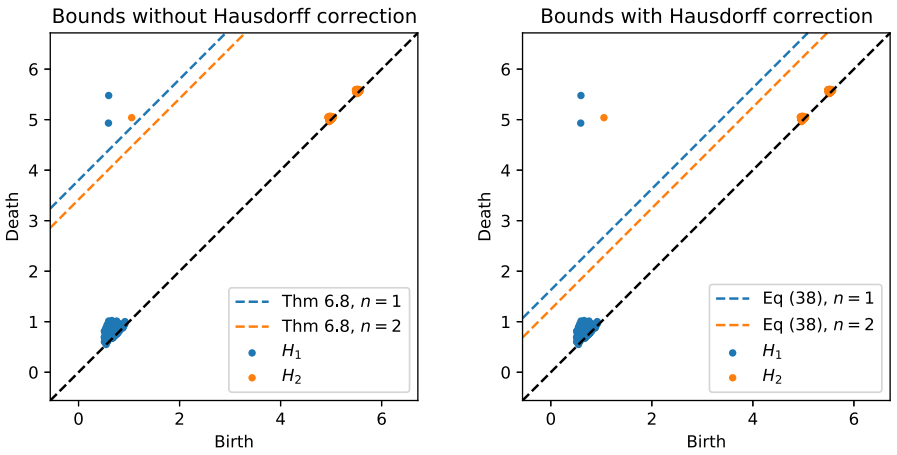

Fig. 10 Rips persistence diagrams of $SW_{d,\tau} f(\widetilde{T})$ in dimensions $j = 1$ (blue) and $j = 2$ (orange), and coefficients in $\mathbb{F} = \mathbb{Z}_2$. Lower bounds on persistence are shown with dashed lines. Left: no Hausdorff correction, and Right: Hausdorff correction (color figure online)

Figure 10 below shows the Rips persistence diagrams $\mathsf{dgm}_j^{\mathcal{R}}(SW_{d,\tau} f(\widetilde{T}))$, as well as the estimated lower bounds in persistence with and without the correction term on Hausdorff distance.

Next, we aim to illustrate the effect of introducing noise to a quasiperiodic signal by examining the sliding window persistence of the resulting signal. Note that in (Tralie and Perea 2018, Section 4.1), the authors extensively studied the effect of adding different types and levels of noise to recurrent videos. They measured the accuracy of a binary classification task inspired by their persistence based (quasi)periodicity scores and showed that persistence separates recurrent and non-recurrent videos under noise very well. Here, we use the function $f(t) = 2\sin(t) + 1.8\sin\left(\sqrt{3}t\right)$ at $t \in T = \left\{\frac{3n\pi}{500} \mid n = 0, \ldots, 9,999\right\}$ and add random Gaussian noise to f. Then we use the Discrete Fourier Transform to determine the frequencies. For parameter selection, we choose d based on the number of prominent peaks and compute the optimal τ as described in Sect. 5.2. For each noise level, we compute the sliding window persistence for 800 landmarks chosen via the `maxmin` subsampling process. In Fig. 11 (Top), we track the maximum persistence (blue) and the second maximum persistence (purple) in dimension 1 as we increase the Noise-to-Signal Ratio (NSR) defined as

$$\text{NSR} = \sqrt{\frac{E[N^2]}{E[S^2]}}$$

where N is the Gaussian noise, S is the signal f, and $E[\,\cdot\,]$ is the expected value. We also show, for contrast, all other lower persistences (gray), i.e. third maximum persistence, fourth maximum persistence, and so on. Similarly, in Fig. 11 (Bottom), we track the maximum persistence (orange) and all other lower persistences (gray), i.e. second maximum persistence, third maximum persistence, etc., in dimension 2.

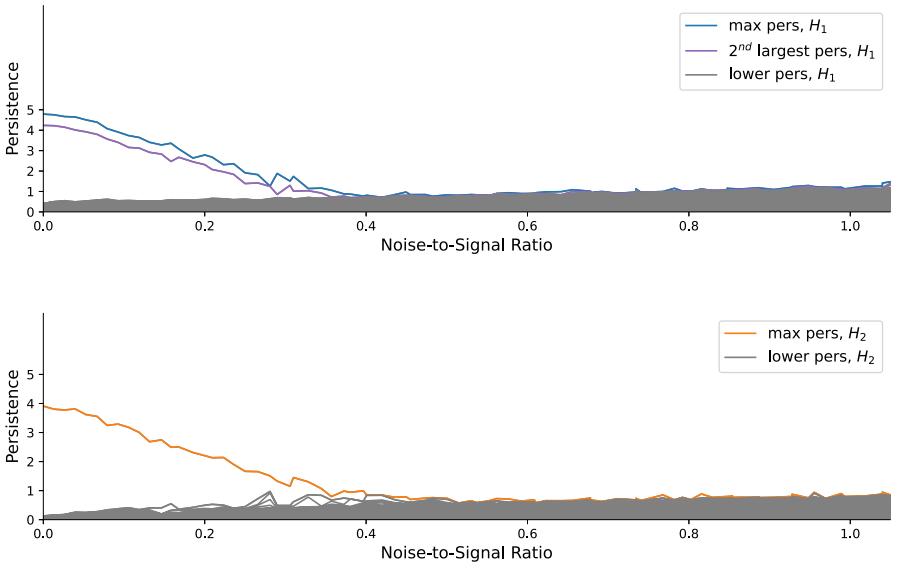

Fig. 11 Sliding Window Persistence versus Noise-to-Signal Ratio. The top figure shows the two maximum persistences in dimension 1 and the bottom figure shows the maximum persistence in dimension 2. In both cases, the curves for lower persistences, i.e. all other persistences are also added for contrast

7.2 Application: dissonance detection in music

In music theory, consonance and dissonance are classifications of multiple simultaneous tones. While the former is associated with pleasantness, the latter creates tension as experienced by the listener. Perfect dissonance occurs when the audio frequencies are irrational with respect to each other. One such instance is the *tritone*, which is a musical interval that is halfway between two octaves. Mathematically, for a base frequency ω_1, its tritone is $\sqrt{2}\omega_1$. We will use the theory of sliding window embedding to quantify quasiperiodicity from a dissonant sample. For the purpose of this application, we use a 5-second audio recording of a brass horn playing the tritone.[1] The signal was read using wavfile.read() and the resulting amplitude plot is shown in Fig. 12 (Top). Like before, in order to perform sliding window analysis, we need to choose appropriate parameters d and τ. We proceed exactly as before with the spectral analysis shown in Fig. 12 (Bottom).

We then find peaks with height at least 0.04 and at least 100 radians per second apart to detect prominent frequencies which we will use for estimation of the embedding parameters. See Table 1.

The resulting embedding parameters are $d = 8$ and $\tau = 0.0285736$. We use cubic splines to compute the sliding window vectors and present the PCA representation of the point cloud, along with the persistence diagrams computed for 1300 landmarks, i.e. `maxmin` subsample as defined in Example 5.2, in Fig. 13.

[1] Generously provided by Adam Huston.

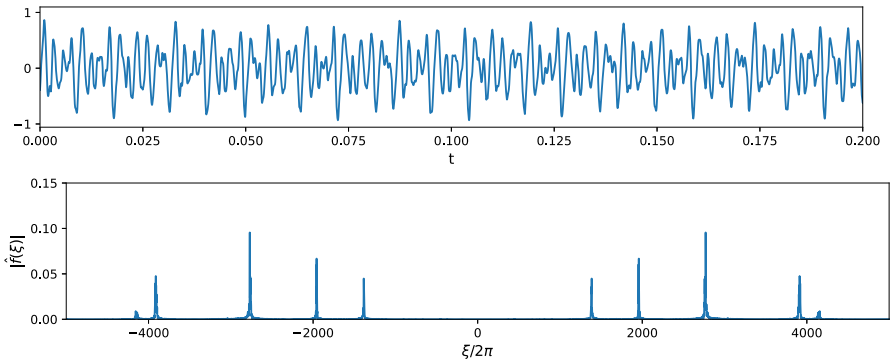

Fig. 12 (Left) The plot of a dissonant music sample created on a brass horn. (Right) The amplitude-frequency spectrum of the music sample plot using Fast Fourier Transform

Table 1 List of frequencies in the positive side of the (symmetric) amplitude-frequency spectrum: First row: list of detected frequencies. Second row: their conversion to Hertz. Third row: ratio with respect to the first row

Angular frequencies	1384.93	1957.83	2769.86	3911.93
Frequencies (Hz)	220.41	311.59	440.83	622.60
Proportion	1	$1.4137 \approx \sqrt{2}$	2	$2.8246 \approx 2\sqrt{2}$

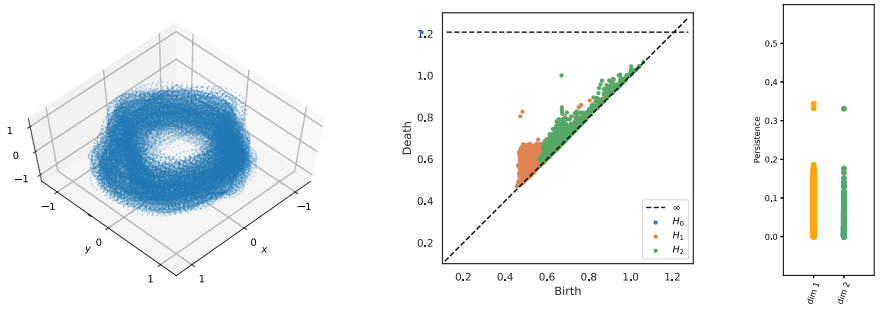

Fig. 13 (Left) PCA representation of the sliding window point cloud. (Middle) Persistence Diagrams in homological dimensions 0, 1 and 2. (Right) The persistence scatter plot

In Fig. 13, the persistence diagrams (middle) indicate that the sliding window point cloud has two high persistence features in dimension 1 and one high persistence feature in dimension 2. This claim is validated with the persistence scatter plot (right). This tell us that the point cloud fills a two dimensional torus (perhaps a very twisted one) embedded in $\mathbb{R}^9$, which verifies that the dissonant music sample was indeed quasiperiodic.

Acknowledgements This work was partially supported by the National Science Foundation through grants DMS-1622301, CCF-2006661, and CAREER award DMS-1943758. The authors of this paper would like to thank Adam Huston for the audio recording of the brass horn. The first author would like to thank Rosemarie Bongers for discussions on some of the Harmonic Analysis aspects of this paper.

Declarations

Conflict of interest On behalf of all authors, the corresponding author states that there is no conflict of interest.

References

Adamaszek, M., Adams, H.: The Vietoris-Rips complexes of a circle. Pac. J. Math. **290**(1), 1–40 (2017)
Apostol, T.M.: Modular Functions and Dirichlet Series in Number Theory, vol. 41. Springer, New York (2012)
Aubel, C., Bölcskei, H.: Vandermonde matrices with nodes in the unit disk and the large sieve. Appl. Comput. Harmonic Anal. **47**(1), 53–86 (2019)
Bauer, U.: Ripser. https://github.com/Ripser/ripser (2016)
Belloy, M., Naeyaert, M., Keliris, G., Abbas, A., Keilholz, S., Van Der Linden, A., Verhoye, M.: Dynamic resting state fMRI in mice: detection of Quasi-Periodic Patterns. Proc. Int. Soc. Magn. Reson. Med. 0961 (2017)
Ben-Israel, A., Greville, T.N.: Generalized Inverses: Theory and Applications, vol. 15. Springer, New York (2003)
Broer, H.: KAM theory: the legacy of Kolmogorov's 1954 paper. Bull. Am. Math. Soc. **41**(4), 507–521 (2004)
Chazal, F., De Silva, V., Oudot, S.: Persistence stability for geometric complexes. Geom. Dedicata **173**(1), 193–214 (2014)
Chazal, F., Crawley-Boevey, W., de Silva, V.: The observable structure of persistence modules. Homol. Homotopy Appl. **18**(2), 247–265 (2016)
Crawley-Boevey, W.: Decomposition of pointwise finite-dimensional persistence modules. J. Algebra Appl. **14**(05), 1550066 (2015)
Das, S., Dock, C.B., Saiki, Y., Salgado-Flores, M., Sander, E., Wu, J., Yorke, J.A.: Measuring quasiperiodicity. Europhys. Lett. **114**(4), 40005 (2016)
Emrani, S., Gentimis, T., Krim, H.: Persistent homology of delay embeddings and its application to wheeze detection. IEEE Signal Process. Lett. **21**(4), 459–463 (2014)
Ferreira, P.J.S.G.: Super-resolution, the recovery of missing samples and Vandermonde matrices on the unit circle. In: Proceedings of the Workshop on Sampling Theory and Applications, Loen, Norway (1999)
Gakhar, H., Perea, J.A.: Künneth formulae in persistent homology. arXiv preprint arXiv:1910.05656 (2019)
Gakhar, H.: A topological study of toroidal dynamics. PhD Thesis. Michigan State University (2020)
Gómez, G., Mondelo, J.-M., Simó, C.: A collocation method for the numerical Fourier analysis of quasiperiodic functions. I: numerical tests and examples. Discrete Contin. Dyn. Syst. B **14**(1), 41 (2010)
Grafakos, L.: Classical Fourier Analysis, vol. 2. Springer, New York (2008)
Hollander, A., Van Paradijs, J.: Quasi-periodic oscillations in TT Arietis. Astron. Astrophys. **265**, 77–81 (1992)
Khasawneh, F.A., Munch, E., Perea, J.A.: Chatter classification in turning using machine learning and topological data analysis. IFAC-PapersOnLine **51**(14), 195–200 (2018)
Laskar, J.: Frequency analysis for multi-dimensional systems. Global dynamics and diffusion. Phys. D Nonlinear Phenom. **67**(1–3), 257–281 (1993)
Moitra, A.: Super-resolution, extremal functions and the condition number of Vandermonde matrices. In: Proceedings of the Forty-seventh Annual ACM Symposium on Theory of Computing, pp. 821–830 (2015)
Morozov, D.: Persistence algorithm takes cubic time in worst case. BioGeometry News, Dept. Comput. Sci., Duke Univ **2** (2005)
Perea, J.A.: Persistent homology of toroidal sliding window embeddings. In: 2016 IEEE International Conference on Acoustics, Speech and Signal Processing (ICASSP), pp. 6435–6439. IEEE (2016)

Perea, J.A.: Topological time series analysis. Not. Am. Math. Soc. **66**(5), 686 (2019)
Perea, J.A., Harer, J.: Sliding windows and persistence: an application of topological methods to signal analysis. Found. Comput. Math. **15**(3), 799–838 (2015)
Perea, J.A., Deckard, A., Haase, S.B., Harer, J.: SW1PerS: sliding windows and 1-persistence scoring; discovering periodicity in gene expression time series data. BMC Bioinform. **16**(1), 257 (2015)
Pollack, J.B., Toon, O.B.: Quasi-periodic climate changes on Mars: a review. Icarus **50**(2–3), 259–287 (1982)
Radovanovic, M., Nanopoulos, A., Ivanovic, M.: Hubs in space: popular nearest neighbors in high-dimensional data. J. Mach. Learn. Res. **11**(sept), 2487–2531 (2010)
Robins, V.: Towards computing homology from finite approximations. In: Topology Proceedings, vol. 24, pp. 503–532 (1999)
Samoilenko, A.M.: Elements of the Mathematical Theory of Multi-frequency Oscillations, vol. 71. Springer, Dordrecht (2012)
Slater, N.B.: Gaps and steps for the sequence n θ mod 1. In: Mathematical Proceedings of the Cambridge Philosophical Society, vol. 63, pp. 1115–1123. Cambridge University Press (1967)
Sós, V.T.: On the distribution mod 1 of the sequence nα. Ann. Univ. Sci. Budapest Eötvös Sect. Math. **1**, 127–134 (1958)
Stein, E.M., Weiss, G.: Introduction to Fourier Analysis on Euclidean Spaces (PMS-32), vol. 32. Princeton University Press, Princeton (2016)
Stewart, I., Tall, D.: Algebraic Number Theory and Fermat's Last Theorem. CRC Press, Boca Raton (2015)
Takens, F.: Detecting strange attractors in turbulence. In: Dynamical Systems and Turbulence. Warwick 1980, pp. 366–381. Springer, Germany (1981)
Tralie, C.J., Berger, M.: Topological Eulerian synthesis of slow motion periodic videos. In: 2018 25th IEEE International Conference on Image Processing (ICIP), pp. 3573–3577. IEEE (2018)
Tralie, C.J., Perea, J.A.: (Quasi)-Periodicity quantification in video data, using topology. SIAM J. Imaging Sci. **11**(2), 1049–1077 (2018)
Tralie, C., Saul, N., Bar-On, R.: Ripser.py: a lean persistent homology library for python. J. Open Source Softw. **3**(29), 925 (2018). https://doi.org/10.21105/joss.00925
Vela-Arevalo, L.V.: Time-frequency analysis based on wavelets for Hamiltonian systems. PhD Thesis. California Institute of Technology (2002)
Webber, C.L., Jr., Zbilut, J.P.: Dynamical assessment of physiological systems and states using recurrence plot strategies. J. Appl. Physiol. **76**(2), 965–973 (1994)
Weixing, D., Wei, H., Xiaodong, W., Yu, C.: Quasiperiodic transition to chaos in a plasma. Phys. Rev. Lett. **70**(2), 170 (1993)
Wilden, I., Herzel, H., Peters, G., Tembrock, G.: Subharmonics, biphonation, and deterministic chaos in mammal vocalization. Bioacoustics **9**(3), 171–196 (1998)
Wojewoda, J., Kapitaniak, T., Barron, R., Brindley, J.: Complex behaviour of a quasiperiodically forced experimental system with dry friction. Chaos Solitons Fractals **3**(1), 35–46 (1993)
Xu, B., Tralie, C.J., Antia, A., Lin, M., Perea, J.A.: Twisty Takens: a geometric characterization of good observations on dense trajectories. J. Appl. Comput. Topol. **3**(4), 285–313 (2019)
Zbilut, J.P., Thomasson, N., Webber, C.L.: Recurrence quantification analysis as a tool for nonlinear exploration of nonstationary cardiac signals. Med. Eng. Phys. **24**(1), 53–60 (2002)